APPLICATION OF SILICON SURFACE-BARRIER DETECTORS TO NEUTRON SPECTROSCOPY

by

John Joseph Keating

A Thesis Submitted to the

Graduate Faculty in Partial Fulfillment of

The Requirements for the Degree of

MASTER OF SCIENCE

Major Subject: Nuclear Engineering

Approved:

Signatures have been redacted for privacy

Iowa State University
Of Science and Technology
Ames, Iowa

1966

TABLE OF CONTENTS

INTRODUCTION

Statement of the Problem

Experimental measurement of the energy spectrum of fast neutrons from monoenergetic and multienergetic neutron sources is a problem which has confronted scientists since the discovery of the neutron in 1932 by Chadwick. Several techniques have been devised for obtaining this information; however, the equipment requirements, time required in taking the measurements, and in some cases the accuracy of the results justifies continuing investigations of the problem.

Determination of the neutron spectrum at points of interest in an operating nuclear reactor places even more stringent requirements on the size of the detecting equipment, its ability to discriminate against gamma rays and other reaction products, and its general response characteristics. The research reported in this work was undertaken to investigate the performance of a relatively simple neutron detection system operating in a reactor environment. The proposed system could also be used for spectrum measurements of monoenergetic sources. The potentially useful range of the system to be discussed is from 0.15 to 2.15 Mev.

General Discussion of Detection System

The detection system discussed in this work consists of a Li^6F "converter" foil (155 $\mu gm/cm^2$ of Li^6F deposited on a 0.020 inch aluminum plate), a silicon surface-barrier semiconductor detector, a charge-sensitive preamplifier, a linear amplifier, and a 400 channel analyzer. The system is shown schematically in Figure 1 and the components are described in Appendix A.

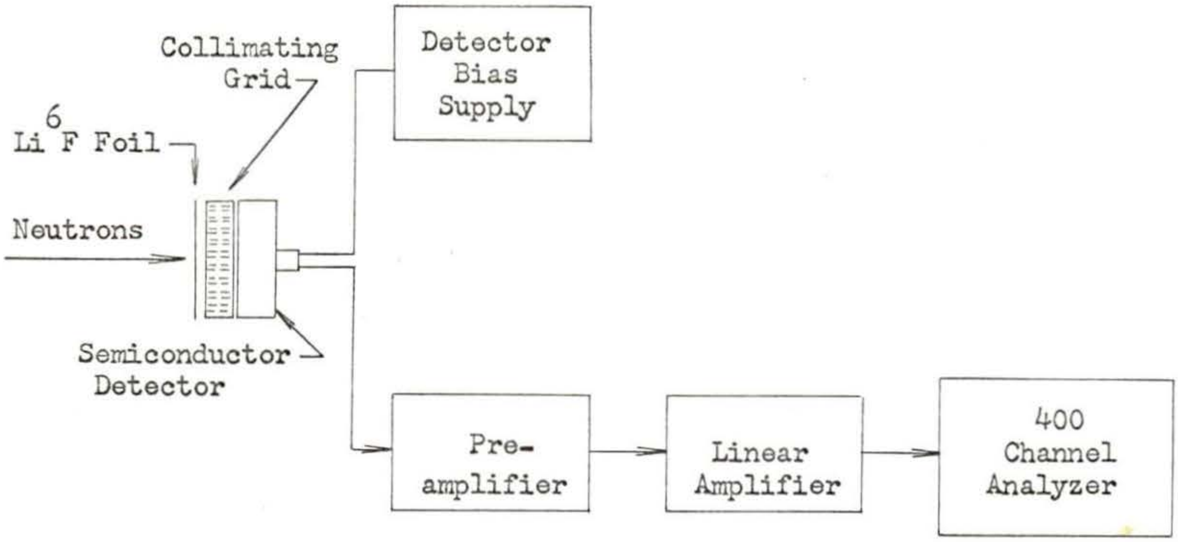

Figure 1. Schematic drawing of detection system

Neutrons of any energy, incident on the "converter" foil, take part in the Li^6 (n,T) He^4 reaction; but the combined energy of triton and alpha particle depends on the incident neutron energy. Since momentum considerations permit only one of the two product particles from a given reaction to reach the detector, it is necessary to selectively detect one particle for study. Tritons produced in the reaction were chosen to be detected by the semiconductor detector. The current pulses produced in the detector are amplified and fed to the 400 channel analyzer where they are sorted and stored in the appropriate channel with pulses of the same magnitude. The counts stored in any given channel represent the total number of counts produced by tritons of a given energy. The alpha particles produced by the Li^6 (n,T) He^4 reaction are prevented from reaching the detector by an aluminum "catcher" or absorber foil placed between the Li^6F foil and the detector. Above a neutron energy of $\sim$2.0 Mev, protons from the

$Al^{27}(n,p)Mg^{27}$ reaction in the aluminum converter plate and grid assembly will provide an unwanted contribution.

The output of the 400 channel analyzer, after background effects are eliminated, is then an energy spectrum of tritons resulting from the $Li^6(n,T)He^4$ reaction. If the Q-value for this reaction, its cross section as a function of neutron energy, and the detection system geometry are known, the energy spectrum of the neutrons that produced the triton spectrum can be calculated. The Q-value of a nuclear reaction is the mass difference (in energy units) between the reactants and the products of the reaction and is 4.78 Mev for the $Li^6(n,T)He^4$ reaction.

The energy of the triton produced in a reaction initiated by a neutron of a given energy is dependent on the angle between its direction of travel and that of the incident neutron. In this work, the physical size of the neutron source (fission foil) and the Li^6F foil, and the distance separating them limits the angle at which the neutrons can be incident on the Li^6F foil. A grid system is placed between the Li^6F foil and the detector to act as a collimator for the scattered tritons. Thus, the maximum triton scattering angle is known, and the maximum and minimum triton energies resulting from a neutron of given energy can be calculated.

A surface-barrier semiconductor detector was chosen as the detecting element for this work. Detectors of this type have a high energy resolution for detection of charged particles yet have a low sensitivity for interaction with neutrons and gamma rays.

History of Semiconductor Nuclear Particle Detectors

The first use of a semiconductor junction device for nuclear particle detection was reported by McKay (20) in 1949. His work indicated that the p-n junction in germanium could be used to detect alpha particles, that the collection time for the charge was quite small, and that the energy required to produce an electron-hole pair in germanium was no more than 3 electron volts. In 1950, Orman et al. (23) did similar work again using germanium p-n barriers as counters. This early work was with detectors of very small effective area and the energy resolution was poor. In 1956, Mayer and Gossick (19) made a small area (6 mm^2) germanium surface-barrier diode which operated at room temperature with rather poor energy resolution, i.e. about 17%. They found the pulse height from this type detector to be proportional to the alpha energy. As early as 1958, semiconductor nuclear particle detectors utilizing the germanium junction at reduced temperatures were being used extensively in nuclear research.

The use of the p-n junction in silicon for detection of nuclear particles was reported in 1959 by McKenzie and Bromley (21) and Mayer (18). These devices, while having the same general operational characteristics as the germanium detectors, had the advantage of more satisfactory operation at room temperature.

Use of semiconductor detector in neutron spectroscopy

The use of semiconductor detectors as the detecting element in neutron spectrometers was first reported in 1961 by Love and Murray (17). The system used involved a 150 $\mu gm/cm^2$ layer of Li^6F sandwiched between two surface-barrier detectors. The electronics system was designed to sum the energy of the alpha particle and triton emitted simultaneously from the

$Li^6(n,T)He^4$ reaction. The output signal was then the sum of the neutron energy (E_n) and the Q-value for the reaction. The reported resolution was 300 Kev full width at half maximum (FWHM) for their detection system.

This design of detector was modified by Dearnaley et al. (5) to make use of the $He^3(n,p)H^3$ reactions. This system utilized two surface-barrier detectors mounted parallel to each other and enclosed in a small steel case which could be filled with He^3 gas at pressures up to 3 atmospheres. A coincidence type electronics system was utilized which summed the proton and triton energy. The coincidence requirement eliminated any counts due to the He^3 recoil. The reported efficiency for this system was about 10^{-5} for 2 Mev neutrons and the energy resolution was 150 Kev FWHM.

Potenza and Rubbino have reported development of neutron spectrometers for use with isotropic neutron sources (24) and neutrons from nuclear reactions and in collimated beams (25). All of these systems use the elastic scattering of protons as the converting reaction and utilize a single silicon surface-barrier detector as the detecting element. These systems were used to measure neutron energies above 2 Mev. The best resolution attained by any of the three systems (at 2 Mev neutron energy) was about 23% for the system designed for use with isotropic sources. That is, the proton spectrum produced by a monoenergetic source of 2 Mev neutrons would have a FWHM of about 0.46 Mev. In all systems, the resolution decreased with reduction in neutron energy below 2 Mev.

A system for reactor flux measurements has been reported by Furr and Runyon (12). This system also uses the elastic scattering of protons as the converting reaction and a single silicon surface-barrier detector as the detecting element. This system had a reported resolution of 50% for neutrons of 0.75 Mev energy and about 10% for neutrons of 2 Mev energy. The resolution below 0.75 Mev dropped rapidly as the neutron energy decreased.

Other Techniques for Neutron Spectrum Measurements

In addition to the nuclear-reaction method and the recoil-nucleus method as discussed previously incorporating semiconductor detectors, other techniques exist for making neutron spectrum measurements. The most common methods are emulsions, scintillation detectors, and time-of-flight.

As discussed in Price (26, p. 352), emulsions utilizing proton recoil are suitable for neutron spectrum measurements in the energy range from about 0.5 to 15 Mev. The lower limit is specified by the short range of the proton tracks while the upper limit is specified by the emulsion thickness. The lower limit can be reduced by loading the emulsion with a material having a positive Q-value for neutron reaction. Li^6 is an example.

The principle disadvantage of the emulsion method is the length of time required to analyze the data.

Scintillation detectors used in this application utilize the converting material as a constituent of the scintillator. Li^6 is the most widely used converting material. Firk et al. (9) have reported the use of a system of this type. The peak produced by thermal neutrons had a resolution of 25%. The resolution for peaks produced by monoenergetic neutrons of higher energy is generally poorer than that for thermal neutrons as can be seen from experimental results published by Murray (22).

This behavior is opposite to that of the surface-barrier detector system.

The use of scintillation detectors for neutron spectroscopy is further limited by their high gamma-ray sensitivity. The principle advantage of this method is the high efficiency attainable.

The time-of-flight technique offers the capability of very good energy resolution but requires a pulsed source of fast neutrons. Firk et al. (10) have reported use of a system which had a total resolution of 40 Kev for neutrons of 2 Mev energy. This system was used to measure neutron energies from 0.5 to 15 Mev.

This technique can, in general, be used to measure neutron energies from thermal to several Mev.

OPERATIONAL ASPECTS OF SILICON SURFACE-BARRIER DETECTORS

The general features of a silicon surface-barrier detector are shown in Figure 2.

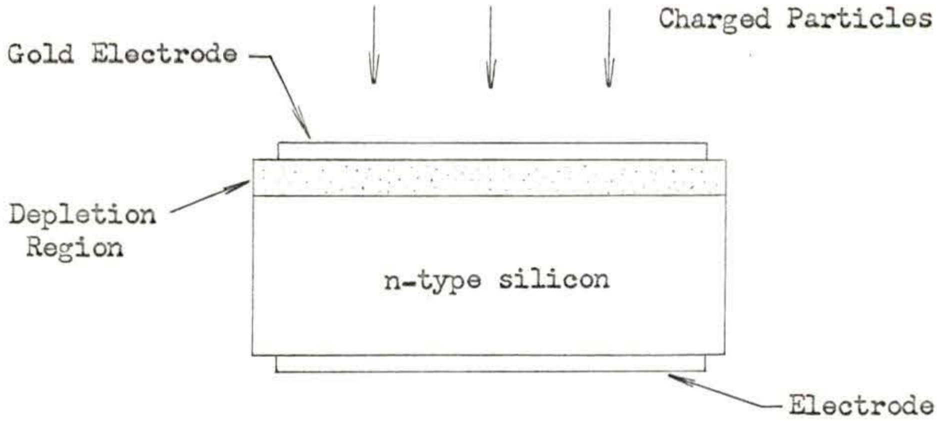

Figure 2. Representation of silicon surface-barrier detector

The bulk material is n-type silicon. On one surface of the bulk material a high density of p-type states is induced with a resulting formation of a p-n junction. On either side of this junction a space charge region or depletion region of high resistivity is set up by diffusion of the electrons from the n-type region into the p-type region and holes from the p-type region into the n-type region. The detection of charged particles takes place in this depletion region.

A charged particle entering the sensitive region of the detector must pass through the thin gold electrode deposited on the surface of the detector. The thickness of this electrode in terms of energy lost by the incident particle is called the window thickness of the detector. The electrode on the back side of the detector is of the nonrectifying type and is bonded to the crystal by a conducting silver paste.

Construction Techniques

Techniques for preparation of surface-barrier detectors are described by several authors including Blankenship and Borkowski (2). Although the various methods differ slightly, they all involve the following essential steps. Zone refined crystals of silicon are cut to the desired size and are smoothed by polishing with submicron-size aluminum oxide or diamond powder. The surface is cleaned by chemically etching with a solvent such as CP4. The p-type surface layer is then allowed to form spontaneously on the n-type silicon by oxidation of the chemically etched surface. This process takes place at room temperature in 12-36 hours and should be conducted in a clean, dust free atmosphere. Maintaining a dust free atmosphere helps to keep foreign materials which may be sources of impurities away from the p-type surface. Following formation of the p-n junction, the edges of the silicon wafer are covered with some type of insulating material (ORTEC uses a ceramic) to prevent breakdown of the junction at the edges of the wafer upon application of an electric field. Electrical contact is made to the p-type surface layer by evaporation of gold in a vacuum usually to 20-50 $\mu gm/cm^2$ in weight. The thickness of gold is not critical and is usually determined by the intended use of the detector, i.e. it would be advantageous to have a thin film of gold for very highly ionized particles such as fission products. Electrical contact is made to the back of the crystal by bonding the crystal to a thin metal plate by use of conducting silver paste. Electrical contact to the front surface-barrier layer is made through a fine gold wire or strip bonded to the gold film by the silver paste.

Formation of Surface-Barrier p-n Junction

The formation of the depletion or space-charge region results from diffusion of the majority carriers when the n-type and p-type materials are brought together. The electrons from the n-type material diffuse toward the p-type material. Diffusion occurs because of the tendency of the carriers to spread to regions of lower density. This diffusion builds up a space-charge region formed on one side by filled electron acceptor sites not accompanied by the required number of holes for zero net charge locally, and on the other side by positively charged empty donor sites not accompanied by equal numbers of electrons in the conduction band required to produce zero net charge. This is illustrated in Figure 3 which represents the band structure as a function of position through a surface-barrier detector. As seen in Figure 3a, a potential difference referred to as the barrier-height potential builds up with the formation of the space-charge. The equilibrium value of this barrier height (V_o) is related to the relative density of holes on the two sides of the junction by the expression

$$V_o = \frac{KT}{e} \ln \left(\frac{p_p}{p_n} \right) \tag{1}$$

where KT is the thermal energy, e is the electronic charge, and p_p and p_n are the hole concentrations in p-type and n-type materials respectively. Typical values of V_o are of the order of 0.5 volts. Application of an external bias positive on the n side and negative on the p side extends the space-charge region as shown in Figure 3b.

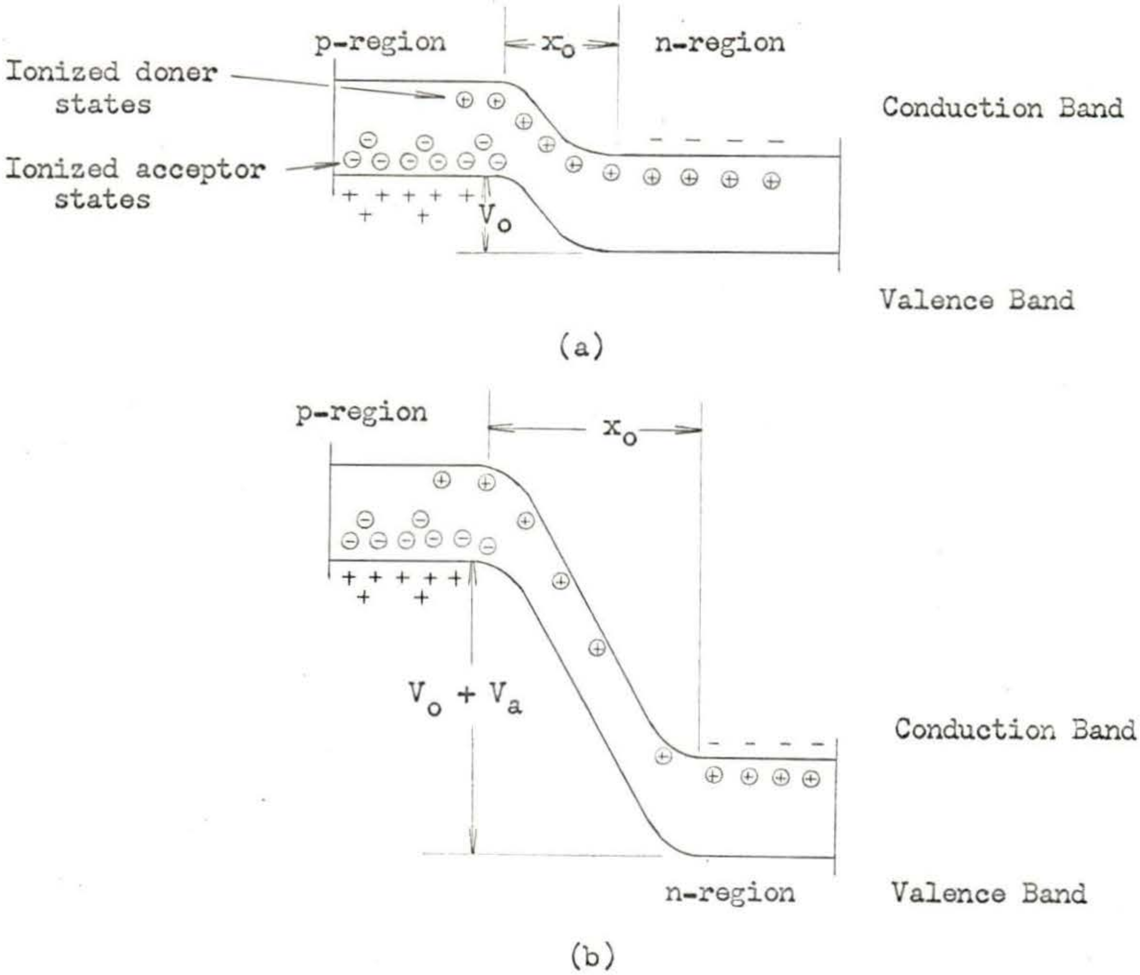

Figure 3. Band structure as a function of position through a surface-barrier detector. (a) no applied bias (b) with reverse bias

The characteristics of the space-charge region can be derived following the approximations of Dearnaley and Northrop (6, p. 127). Figure 4 shows the p-n system characteristic of surface-barrier devices and defines the nomenclature for derivation of the space-charge relationships.

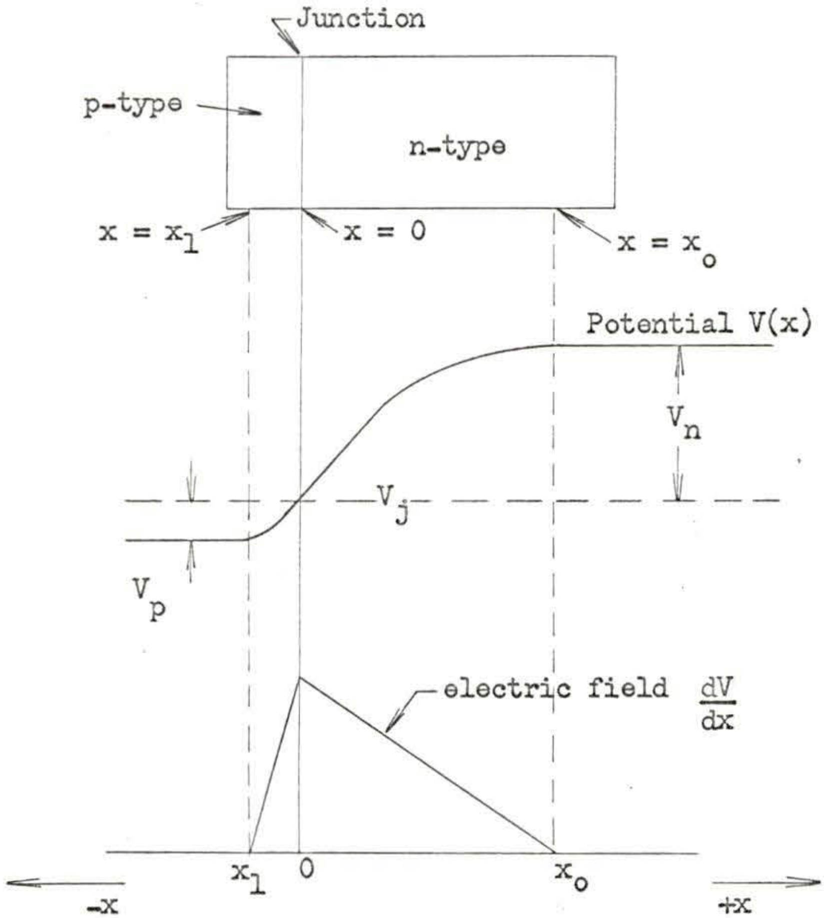

Figure 4. Definition of nomenclature for derivation of space-charge relationships

The assumptions made by Dearnaley are the following:

a. All acceptors in the p-type region are ionized up to x_1, and all donors in the n-type region are ionized up to x_o.

b. Beyond x_o and x_1 the electric field is assumed to be zero.

c. The presence of acceptors in the n-type region and of donors in the p-type region is neglected.

By Poisson's relation, in the n-type region

$$\frac{d^2 V}{d x^2} = - \frac{4 \pi n_n e}{K_o} \qquad (2)$$

and in the p-type region

$$\frac{d^2 V}{d x^2} = \frac{4 \pi p_p e}{K_o} \qquad (3)$$

where K_o is the dielectric constant of silicon and n_n is the electron concentration in n-type region. Considering the n-type region, successive integrations using the above boundary conditions yields

$$\frac{d V}{dx} = - \frac{4 \pi e n_n}{K_o} (x - x_o) \qquad (4)$$

and

$$V (x) = - \frac{2 \pi e n_n}{K_o} (x^2 - 2x x_o) + V_j \qquad (5)$$

When $x = x_o$, $V (x) - V_j = V_n$ and the above equation becomes

$$x_o^2 = \frac{V_n K_o}{2\pi n_n e} \tag{6}$$

Similarly the extension into the p region is found to be

$$x_1^2 = \frac{V_p K_o}{2\pi p_p e} \tag{7}$$

On the basis of the model used, the excess charge in the n-type material is equal and opposite to that in the p-type region since the field is confined to the space-charge region in this approximation. Therefore,

$$n_n x_o = p_p x_1 \tag{8}$$

and the depletion region is seen to penetrate the two regions in the inverse ratio of their ionized impurity states. For surface-barrier detectors $p_p / n_n \gg 1$ and as a result the depletion region exists almost completely in the n-type region. The square of the depletion region width is then approximately

$$x_o^2 = \frac{(V_o + V_a) K_o}{2\pi n_n e} \tag{9}$$

where V_o is given by Equation 1 and V_a is the externally applied voltage. If all the donors in the space-charge region are ionized, the resistivity of the material is

$$\rho = \frac{1}{n_n e \mu_n} \qquad (10)$$

where μ_n is the electron mobility in the n-type region. Substitution of Equation 10 into Equation 9 yields for the depletion region width

$$x_o = \left[\frac{K_o \mu_n}{2\pi} \rho (V_o + V_a) \right]^{\frac{1}{2}} \qquad (11)$$

Thus it is seen, the depletion region width for a given resistivity detector is a direct function of the applied voltage.

Electron-Hole Production in Semiconductors

When a charged particle passes through a solid medium, it loses its energy through interactions with the electrons in the medium. If the medium is a semiconductor material, this interaction results in the formation of electron-hole pairs, i.e., an electron, originally in the valence band or possible some lower lying occupied electronic band, is excited to the conduction band or some higher unoccupied band leaving at the point of interaction a net positive charge or hole. For silicon, the average value of energy required to produce an electron-hole pair, (designated as ϵ), has been found by Mayer (18), to be 3.50 ev. As far as is known, ϵ is independent of both the mass and energy of the charged particle.

If the charged particle has mass M_p and energy E_p, the maximum energy

(E_{max}) that can be transferred to an electron of mass m_e is given by

$$E_{max} = \frac{4 \; m_e M_p}{(m_e + M_p)^2} \; E_p \qquad (12)$$

If $M_p \gg m_e$, and since even for a proton $M = 1836 \; m_e$, the maximum energy transfer becomes approximately

$$E_{max} \cong \frac{4 \; m_e E_p}{M_p} \qquad (13)$$

which will be about 2.9 Kev for a 4 Mev triton. Since the width of the energy gap in silicon is 1.106 electron volts, it is seen that these energy loss processes can lift electrons from the valence band or lower lying occupied energy bands to the conduction band or higher lying unoccupied bands, and holes are found in bands which are normally filled with electrons. During the transition from the excited states, many more electron-hole pairs are produced with the average energy required for production of each pair being the ϵ discussed previously. The total number of electron-hole pairs produced by a given charged particle is thus directly proportional to the energy of the particle. If an electric field is being applied to the semiconducting material during this time, the electron in the conduction band will move under the influence of the field, and likewise, the hole will be passed from atom to atom. This transfer of charge within the medium can be used as an indication of the amount of energy deposited within the medium if the average energy required to produce an electron-hole pair is known.

Charge Collection

To illustrate how the electrons and holes are collected within the detector and the resulting pulse is formed, consider the counting circuit shown in Figure 5.

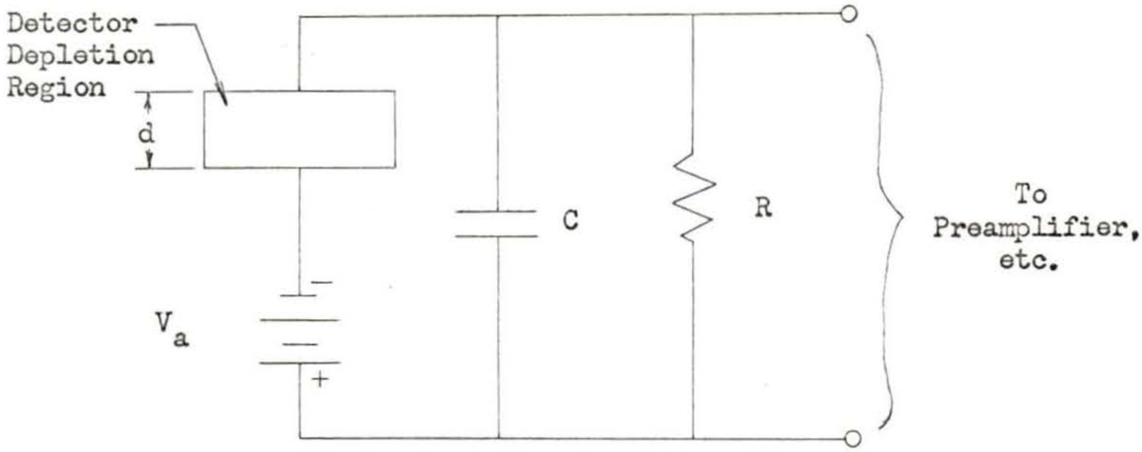

Figure 5. Schematic drawing of detector circuit

The signal in the circuit external to the detector builds up as the electrons and holes are swept out of the depletion region by the electric field present. Each electron contributes a current ev / d when moving with a velocity v in the counter and produces an identical current in the external circuit. The signal is made up of current pulses from both electrons and holes, and any electron causes a charge to flow in the external circuit $\int \frac{ev}{d}\,dt$ integrated over the total path of the carrier. If the carrier traverses the counter completely, the limits of integration are zero and d / v, and the integral reduces to e. If the carrier drift length λ is less than the specimen dimension, the charge flowing in the external circuit is reduced proportionately to $e\lambda / d$. The transit time for each of the carriers is given by

$$\tau_c = \frac{d}{\mu \mathcal{E}} \tag{14}$$

where μ is the mobility of the carrier being considered and $\mathcal{E} = \frac{V_a}{d}$, i.e. the electric field strength in the depletion region.

In a detector in which there is no trapping or recombination, a particle which generates a total of N ion pairs at a distance x from the negative electrode will give a total charge of Ne flowing through the external circuit. Of this, the holes will contribute a charge $q_h = \frac{Nex}{d}$ in a time $\tau_h = \frac{x}{\mu_p \mathcal{E}}$ and the electrons will contribute a charge $q_e = Ne \frac{(d-x)}{d}$ in a time $\tau_e = \frac{d-x}{\mu_n \mathcal{E}}$.

Window Thickness

As can be seen from Figure 2 (p.8), a particle must pass through an insensitive region or window before it reaches the depletion region of a surface-barrier detector. Particles lose energy in passing through this window, and an account must be made of this. For surface-barrier detectors, Dearnaley and Whitehead (7) have found that the window thickness is essentially the thickness of gold film required to provide electrical contact with the p-type material. The thickness of this gold film is 20 to 50 μgm/cm^2 by weight. This small window thickness for surface-barrier detectors is one of their principle advantages over other kinds of semiconductor detectors such as the diffused junction and ion-drifted types.

This is especially true when the detector is being used for energy measurements of highly ionized particles. The detector used in this work is specified by the manufacturer to have a dead layer of thickness not exceeding $40 \mu gm/cm^2$. This corresponds to an energy loss of 20 Kev for a 5.5 Mev alpha particle.

Sensitivity to Gamma Rays

Interaction of gamma rays with silicon and the surrounding material results in the production of Compton electrons, photoelectrons, and electron-positron pairs. The cross section for these processes is proportional to $\frac{Z}{E_\gamma}\left[\ln \frac{2 E_\gamma}{.51 \text{ Mev}} + \frac{1}{2}\right]$, $Z^5 (E_\gamma)^{-3.5}$, and $Z^2 (E_\gamma - 1.02 \text{ Mev})$ respectively, where E_γ is gamma ray energy in Mev and Z is the atomic number of the material in which the processes are taking place. Because of the low atomic number of silicon, the photoelectric process and pair-production are unfavored. In the case of a shallow barrier such as a surface-barrier, the sensitive volume is so thin that electrons lose negligible energy before escaping from it and thus gamma rays produce only small pulses with low efficiency. The size of the pulses produced by gamma interaction makes it easy to discriminate against them.

Sensitivity to Neutrons

Neutrons can produce pulses in surface-barrier detectors by undergoing charged-particle reactions with the silicon itself. The known reactions, their Q-values, percentage abundance of the various isotopes of silicon, and the reaction cross section at various neutron energies are shown in Table 1. This data is from Dearnaley (4).

Of the known reactions, the Si^{28} (n,p) Al^{28} reaction is the most significant due to the high abundance of Si^{28} and the relatively large cross section for the reaction. Its effect in producing background counts must be considered when doing counting in the presence of high energy neutrons. The probability of neutron reactions in the gold window, resulting in the release of charged particles, is extremely small due to the large "coulomb" barrier of the gold nucleus.

Table 1. Neutron reactions in silicon

Reaction	Percent Abundance of Silicon Isotope (%)	Reaction Q-Value (Mev)	Neutron Energy (Mev)	Reaction Cross Section (barns)
$Si^{28}(n,p)Al^{28}$	92	-3.86	5	0.02
			8	0.40
			14	0.22
$Si^{28}(n,\alpha)Mg^{25}$	92	-2.66		
$Si^{29}(n,p)Al^{29}$	4.70	-3.20	14	0.10
$Si^{30}(n,\alpha)Mg^{27}$	3.10	-4.19	14	0.05
$Si^{29}(n,\alpha)Mg^{26}$	4.70	-0.0215		

Energy Resolution

The resolution of a detection system is a measure of the extent to which monoenergetic particles produce pulse heights or charge pulses of a single value. The degree of uniformity of pulse heights is usually described by the quantity $W_{\frac{1}{2}}$, the full width at half maximum (FWHM). The quantity $W_{\frac{1}{2}}$ is calculated as

$$W_{\frac{1}{2}} = \frac{\Delta h_{\frac{1}{2}}}{h_{max}} \times 100\% \qquad (15)$$

where h_{max} is the pulse height corresponding to the maximum in the curve and $\Delta h_{\frac{1}{2}}$ is the pulse height interval between the points at which one half of the maximum occurs.

The several factors which affect the energy resolution of semiconductor detectors have been grouped into three categories by Price (26, p.249). These are the statistics of electron-hole formation, the detector and amplifier noise, and miscellaneous other effects to be discussed later.

The contribution of the statistics of electron-hole formation to the spread in pulse height, expressed in terms of energy, is given by

$$W_1 = 2.36\, \xi_{E_p} \qquad (16)$$

where ξ_{E_p} is the standard deviation in the amount of energy dissipated in the detector by a particle of known energy (E_p). This can also be written as

$$W_1 = 2.36(N)^{\frac{1}{2}}\epsilon = 2.36(E_p \epsilon)^{\frac{1}{2}} \qquad (17)$$

where ϵ is the energy required on the average to produce an electron-hole pair and N is the number of ion pairs formed, i.e., E_p / ϵ on the average for each particle of energy E_p.

In this work, the detector and amplifier noise and the miscellaneous effects are determined experimentally as one contribution to the detection system energy resolution. This is discussed later.

Radiation Damage

Significant deterioration of the properties of semiconductor detectors is produced by extensive irradiation. Interaction of the nuclear radiation with the nuclei of the semiconductor causes atoms to be displaced from their equilibrium positions leaving vacancies and interstitial atoms in the lattice. These imperfections act as trapping centers for the charge carriers, i.e., an electron originally in the conduction band can fall into a trapping center located between the valence and conduction bands of silicon. The electron will remain at the trapping site for a finite time and then go back into the conduction band. A similar process takes place for holes. These trapping centers cause an increase in the charge-carrier generation and a reduction in the charge-carrier lifetime. The resulting changes in detector properties include increased pulse rise time, lower charge collection efficiency, and decreased resolution due to increased leakage current.

The effect of fast (fission) neutrons on surface-barrier detectors has been reported by Klingensmith (16). In his work, seven silicon surface-barrier detectors were exposed to a U^{235} fission neutron spectrum, and the damage effects were observed by measuring changes in the detector response to Pu^{239} alpha particles. After an exposure of $\sim 3 \times 10^{11}$ neutrons/cm^2 the low energy side of the alpha peak showed a secondary peak. With increasing dose, the original peak broadened but maintained a constant pulse height while the secondary peak decreased in pulse height and became very broad. The total counting rate remained constant with the counts being shared between the two peaks. After 2×10^{12} neutrons/cm^2, the original single peak response was no longer evident. Over the range of dose from 10^{12} to 10^{13} neutrons/cm^2, the reverse current of the detectors, i.e. the current flowing across the depletion-region in the absence of ionizing radiation, increased by an order of magnitude. The resistivities characteristic of the detectors involved in this work were high (3000 ohm - cm, n-type) and the bias voltages were low (6 volts) so that the collecting field was low and the effects of the trapping centers may be expected to be particularly noticeable.

Dearnaley (4) exposed several detectors of around 1000 ohm - cm silicon to a high flux of 5.5 Mev alphas and studied the effects of the resulting damage. After 10^8 alphas/cm^2 a slight decrease in reverse current was observed at a detector bias of 2 volts. The detector resolution began to deteriorate after 2×10^9 alphas/cm^2 and multiple peaking was evident. After 10^{11} alphas/cm^2 the resolution in the different detectors had deteriorated from 1.5% (undamaged) to between 6% and 15% at 2 volts bias. At a bias of 20 volts, the resolution increased to only 3-4% and multiple peaking was never apparent.

DETECTION SYSTEM ANALYSIS

The detection of any nuclear particle requires that the particle undergo some type of interaction with the detection element. For charged particles being detected by semiconductor detectors, this process involves the production of electron-hole pairs as the particle loses its energy in passing through the semiconductor material. The mechanism primarily responsible for the energy loss by the particle is the interaction of the coulomb fields of the particle with those of the bound electrons of the absorber. Since neutrons have no charge there will be no coulomb forces with orbital electrons. As a result, the detection and determination of the energy of neutrons requires a secondary reaction in which the neutron interacts with a given nuclide and produces a charged particle whose energy is dependent on the neutron energy. In this work, the $Li^6(n,T)He^4$ reaction was used. The relevant Q-value is 4.78 Mev.

The $Li^6(n,T)He^4$ reaction takes place in a "converter foil" of Li^6F. This foil is 155 μ gm/cm^2 thick of 300 mm^2 surface area and is deposited on an aluminum disk 0.020 inches thick. The cross section for this reaction as a function of neutron energy is shown in Figure 6.

The particles produced in the $Li^6(n,T)He^4$ reaction are collimated by a grid assembly of aluminum such that only those particles which are scattered within certain angular limitations will reach the detector. At the center of the grid is an aluminum foil (4.83 mg/cm^2) which acts as a filter for these particles, i.e., it passes the tritons after reducing their energy by a known amount but effectively absorbs all alpha particles. While the foil does not completely stop high energy alpha particles, it

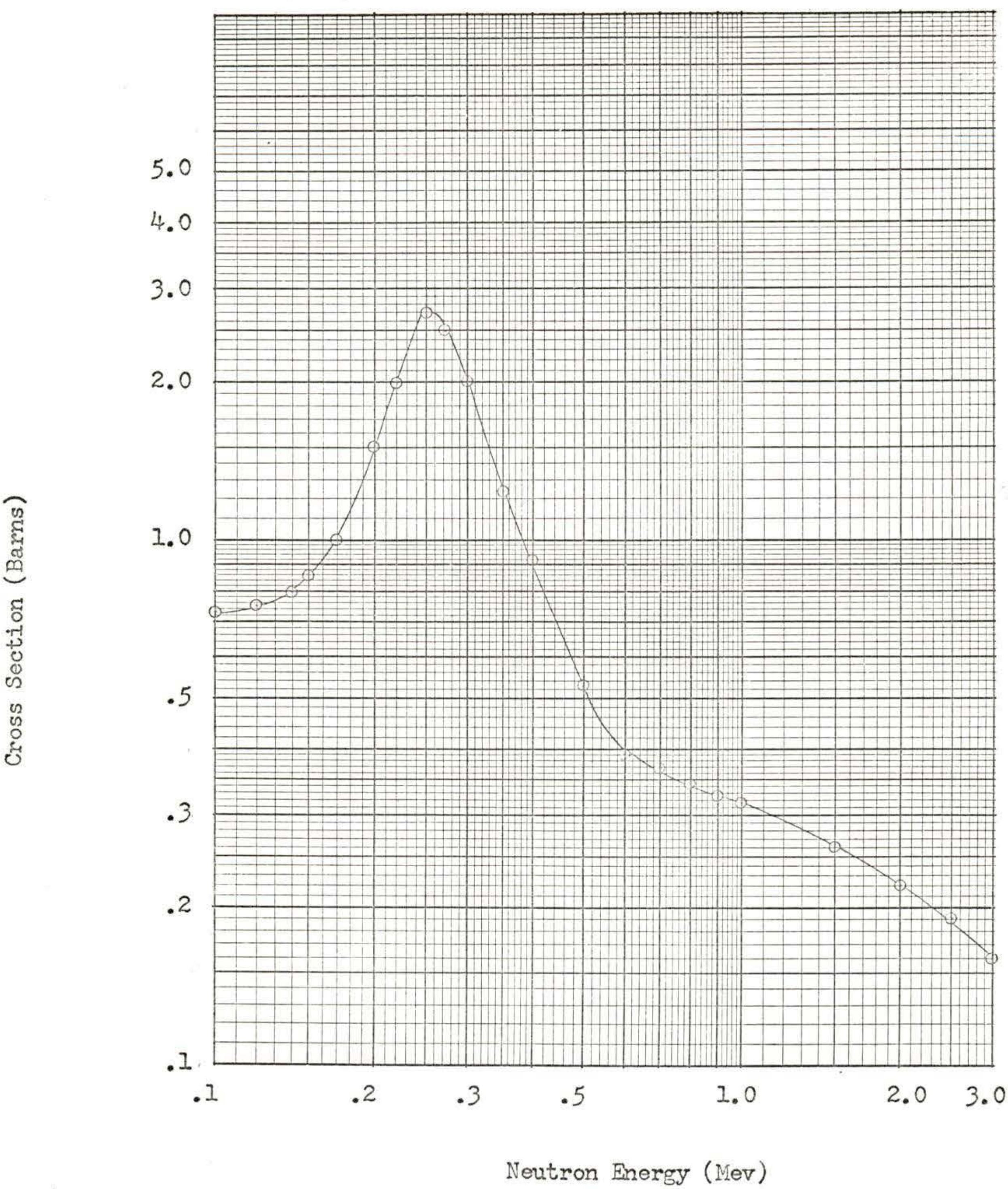

Figure 6. Cross section vs neutron energy for $Li^6(n,T)He^4$ reaction

reduces their energy to the point that they are not in the energy range of interest.

Detection System Geometry

The fission plate, "converter" foil, grid with alpha particle "catcher", and the detector are positioned as shown in Figure 7. The fission plate is 1 inch in diameter, 0.020 inches thick and is located 2 inches from the Li^6F "converter" foil. The "converter" foil is separated from the detector surface by 0.135 inches of which 0.123 inches is occupied by the grid. The grid is constructed of two disks of 0.060 inch aluminum through which have been drilled 51 matching holes of 0.082 inch diameter. The aluminum "catcher" foil is placed between the two halves of the grid. The web of the grid reduces the useful area of the detector from 300 mm^2 to 174 mm^2.

The system geometry is in part dictated by the dynamics of the $Li^6(n,T)He^4$ reaction, i.e., it is necessary to limit the angle at which tritons can be scattered (with respect to the direction of neutron travel) and still be detected in order that the system resolution chosen can be limited to acceptable values. It will be shown that the energy of the scattered triton is dependent on the scattering angle in the center-of-mass system which in turn depends on the scattering angle in the laboratory system. From Figures 7 and 8 it is seen that the maximum angle at which a triton can be scattered in the laboratory system and still be detected by this system is 55 degrees.

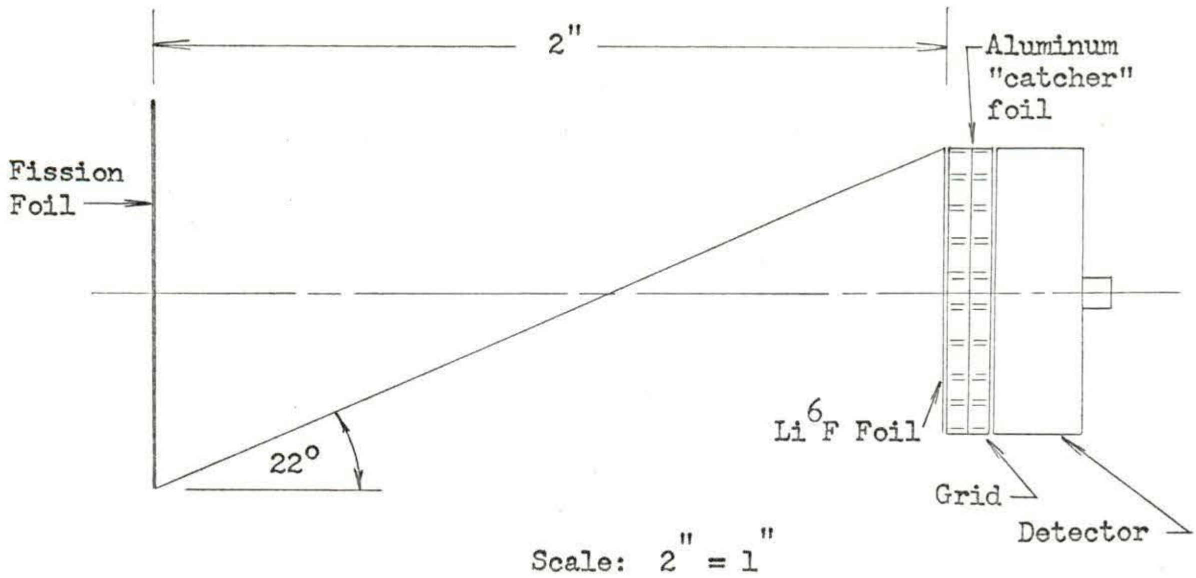

Figure 7. Detection system geometry

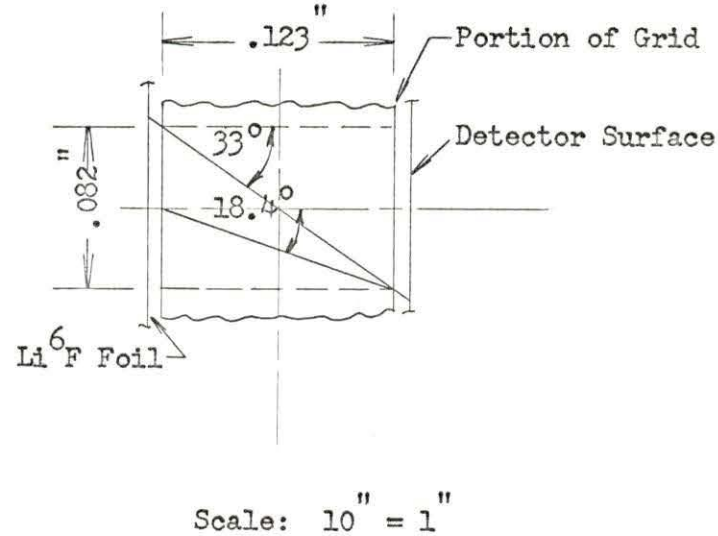

Figure 8. Detail of grid hole

Dynamics of the $Li^6(n,T)He^4$ Reaction

The dynamics of the $Li^6(n,T)He^4$ reaction are governed by the laws of conservation of energy and momentum. The following treatment is similar to that of Keepin and Roberts (15). Interaction of the neutron with the Li^6 atom produces a Li^7 compound nucleus which disintegrates to form an alpha-particle and a triton of energies E_α and E_T respectively. The particle energies are considered to be entirely kinetic since there are no excited states of tritium in the energy range of interest.

The reaction as it would appear in the center-of-mass coordinate system and in the laboratory coordinate system is shown in Figures 9a and 9b respectively. A comparison of Figure 9b with Figures 7 and 8 reveals that ϕ has a maximum value of 55°.

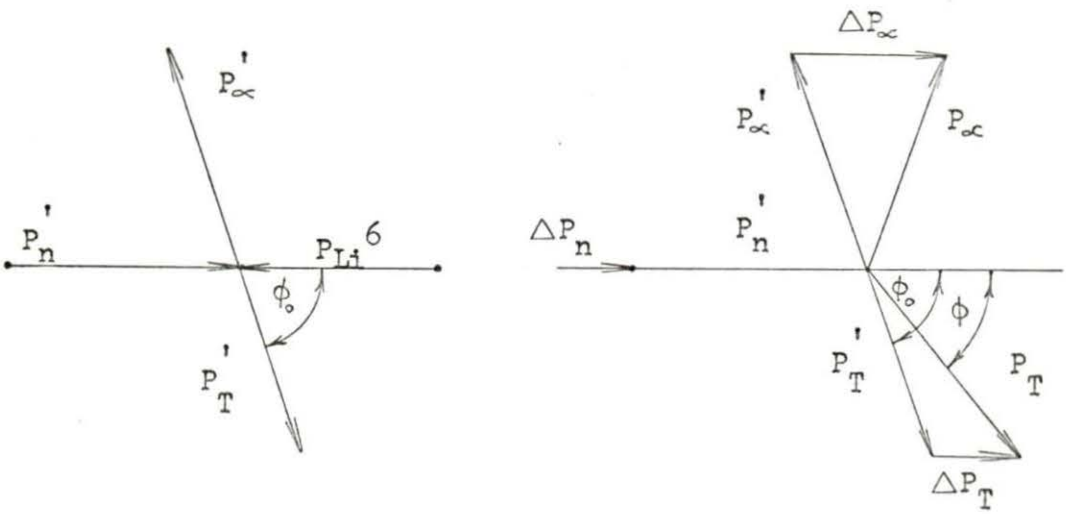

(a) Center of mass system (b) Lab system

Figure 9. Dynamics of the $Li^6(n,T)He^4$ reaction

The energy available for distribution between disintegration products in the center-of-mass system is

$$E_{dp} = E_n + Q - \left[\frac{m_n}{m_n + M} \right] E_n$$

where m_n is the neutron mass and M the mass of the Li^6 nucleus. The remaining energy, of magnitude

$$\left[\frac{m_n}{M + m_n} \right] E_n$$

goes into the kinetic energy of the center-of-mass. The alpha-particle and the triton divide the energy E_{dp} in their inverse mass ratio and their respective momenta are given by

$$P'_\alpha = P'_T = \left[\frac{2\, m_\alpha\, m_T}{m_\alpha + m_T} \left(\frac{M\, E_n}{m_n + M} + Q \right) \right]^{\frac{1}{2}} \qquad (18)$$

Motion of the center-of-mass in the laboratory system adds, in effect, the components ΔP_α, ΔP_T, and ΔP_n whose magnitudes are given by the particle mass times the velocity of the center-of-mass.

The relationship between the triton scattering angle in the center-of-mass system and in the laboratory system is seen from Figure 9b to be

$$\tan \phi = \frac{P'_T \sin \phi_o}{P'_T \cos \phi_o + \Delta P_T} \qquad (19)$$

Again from the geometry as seen in Figure 9b, we have the vector relation

$$\overline{P_T} = \overline{P'_T} + \overline{\Delta P_T} \qquad (20)$$

The triton energy is then given by (21)

$$E_T = \frac{1}{2m_T}\left[\left(P_T'\right)^2 + \left(\Delta P_T\right)^2 + 2\,P_T'\Delta P_T' \cos\phi_o\right]$$

From Equation 21 it is seen that for a neutron of a given energy, the triton can have a range of values of energy depending on the angle between the direction of the incident neutron and the direction in which the triton is scattered from the point of the Li^7 nucleus disintegration in the center-of-mass system. If the neutron energy is to be found from experimental measurements of triton energies, it is necessary to limit the triton scattering angle in order that the neutron energy can be determined within known limits. In this system, the triton scattering angle is limited by the geometry of the experiment to be less than $\phi = 55^\circ$ in the lab system (or less than ϕ_o in the center-of-mass system). Since the range of triton energies is dependent on ϕ_o, this angle must be calculated. Equation 19 is used for this purpose. When ϕ_o is known for each incident neutron energy, it is possible to calculate the range of permitted triton energies due to the system geometry and the dynamics of the $Li^6(n,T)He^4$ reaction. The results of these calculations are shown in Table 2. As seen in Table 2, a 0.15 Mev neutron can produce a detectable triton whose energy will be in the range from 3.00 to 3.11 Mev corresponding to values of ϕ_o of 57.9° and 0° respectively. Since the neutron can be incident to the Li^6F foil at any angle between 0 and 22 degrees and the triton can be scattered at any angle between 0 and 33.0 degrees in the laboratory system, it is assumed the most probable triton energy will be the mean of the maximum and minimum allowed values of 3.055 Mev

Table 2. Range of triton energies permitted by system geometry and $Li^6(n,T)He^4$ reaction dynamics

Neutron Energy (Mev)	ϕ (degrees)	ϕ_o (degrees)	$(P'_T)^2$ $\times 10^{+29}$	$(\Delta P_T)^2$ $\times 10^{+31}$	$2P_T \Delta P_T$ $\times 10^{+30}$	$2P'_T \Delta P_T \cos\phi_o$ $\times 10^{+30}$	$(E_T)_{min}$ (Mev)	$(E_T)_{max}$ (Mev)
0.150	55	57.90	4.520	1.467	5.145	2.730	3.000	3.110
0.200	55	58.10	4.540	1.965	5.975	3.160	3.041	3.194
0.258	55	58.25	4.590	2.522	6.800	3.580	3.100	3.270
0.270	55	58.30	4.600	2.635	6.960	3.650	3.110	3.290
0.300	55	58.50	4.625	2.940	7.360	3.840	3.140	3.355
0.350	55	58.80	4.660	3.405	7.980	4.140	3.182	3.396
0.400	55	59.25	4.700	3.920	8.590	4.395	3.230	3.460
0.565	55	60.00	4.820	5.530	10.320	5.160	3.362	3.650
0.600	55	60.25	4.860	5.870	10.600	5.300	3.400	3.700
1.100	55	61.60	5.240	10.810	15.070	7.160	3.784	4.240
1.500	55	62.50	5.560	14.720	18.100	8.350	4.080	4.660
2.000	55	63.50	5.960	19.600	21.600	9.640	4.440	5.150
2.150	55	63.90	6.080	21.150	22.670	9.990	4.560	5.300

for a 0.15 Mev neutron.

It is noted, the selection of 55 degrees as the maximum permissible triton scattering angle is the result of a compromise between the energy resolution and the efficiency of this detection system.

Triton Energy Losses

A triton produced in the "converter" foil loses energy in that foil, in air, in the aluminum "catcher" foil, and in the gold layer on the detector surface prior to reaching the sensitive volume of the detector. After leaving the converter foil, the triton must travel through 0.186 mg/cm^2 of air, 4.83 mg/cm^2 of aluminum, 0.23 mg/cm^2 of air, and then pass through the gold layer on the detector surface.

Triton energy losses in the "converter" foil and in the detector "window" are small (i.e. $\sim$3.5%) compared to the energy losses in the air and the aluminum and are not accounted for in this analysis.

Triton energy losses in air and aluminum were determined using curves of dE/dx vs triton energy for the respective media. These curves are shown in Figures 10 and 11. Figure 10 was drawn from data presented by Aron et al. (1). Figure 11 was drawn from data presented by Wolke et al. (28) and Kahn (14).

For energy losses in air, the value of dE/dx was assumed constant during the energy loss process and thus the reduction in triton energy was calculated as the product of dE/dx in $Kev/mg/cm^2$ (at the appropriate value of triton energy) and the density thickness of the air in mg/cm^2. The error due to this assumption being $\sim$0.9 Kev for tritons produced by thermal neutron interaction.

Triton energy losses in aluminum were calculated assuming the rate of energy loss to be linear during the energy loss process, i.e., the value of dE/dx was assumed to be of the form

$$+ \frac{dE_T}{dx} = mE_T' + b \tag{22}$$

where $\frac{dE_T}{dx}$ is the average rate of energy loss by the triton in the aluminum "catcher" foil, E_T' is the appropriate triton energy, m is the slope of the appropriate part of the curve shown in Figure 11, and b is the intercept of the straight line (of slope m) with the ordinate at 0 triton energy.

This assumption was necessitated by the fact that the conventional energy loss equations are not valid in this low range of triton energies, and it was necessary to use experimentally determined energy loss data.

The values of m, E_T' and b were determined for each value of neutron energy as follows:

1. The triton energy just prior to its entering the "catcher" foil was taken to be the mean of its maximum and minimum values calculated considering system geometry effects minus its energy loss in passing through 0.060 inches of air.
2. Using this value of triton energy and the value of dE/dx corresponding to it, an initial calculation of triton energy loss was made assuming the triton to be normally incident to the "catcher" foil.
3. m was then determined by drawing a straight line through the points on Figure 11 corresponding to the triton energy just prior

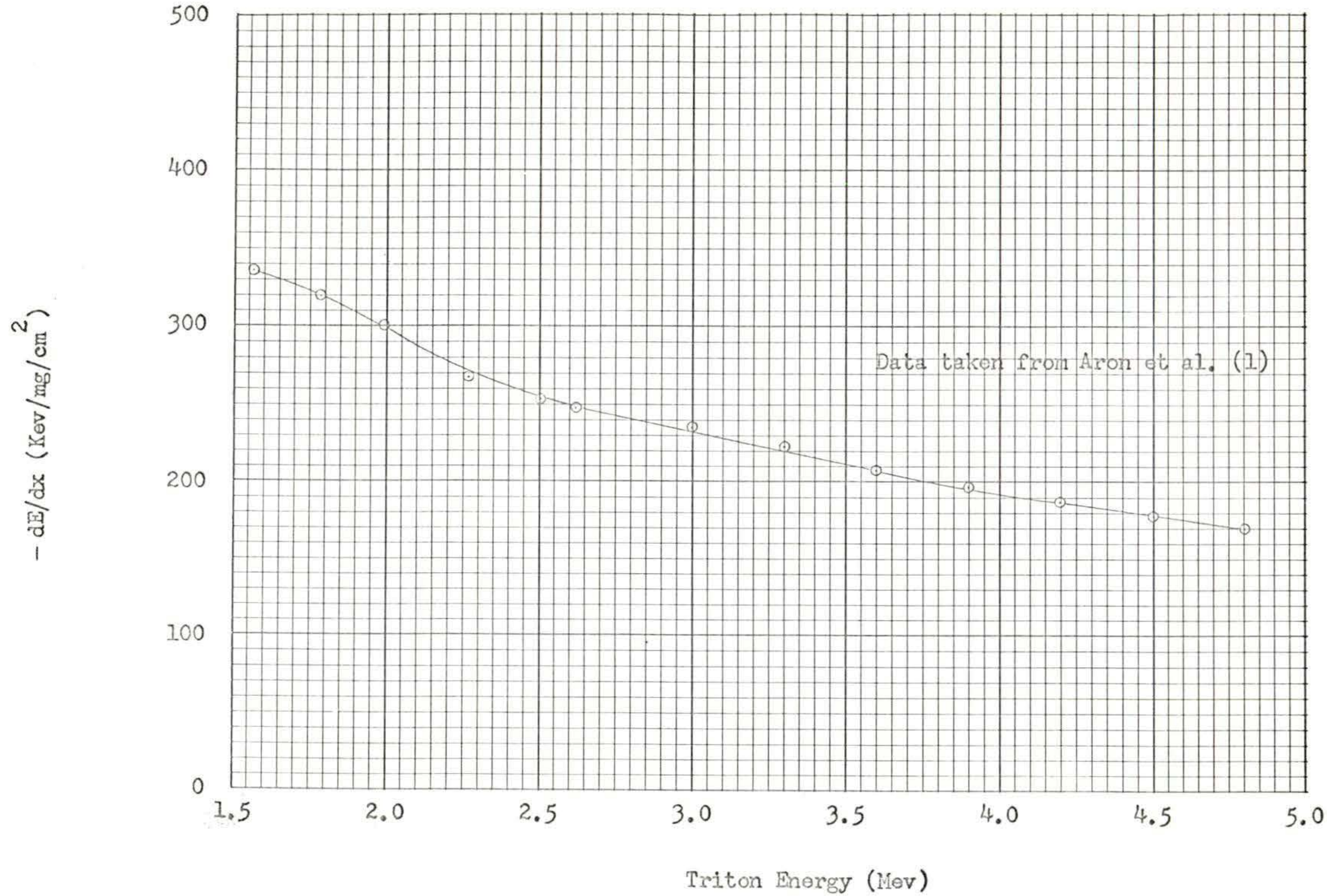

Figure 10. Specific energy loss of tritons (in air) vs triton energy

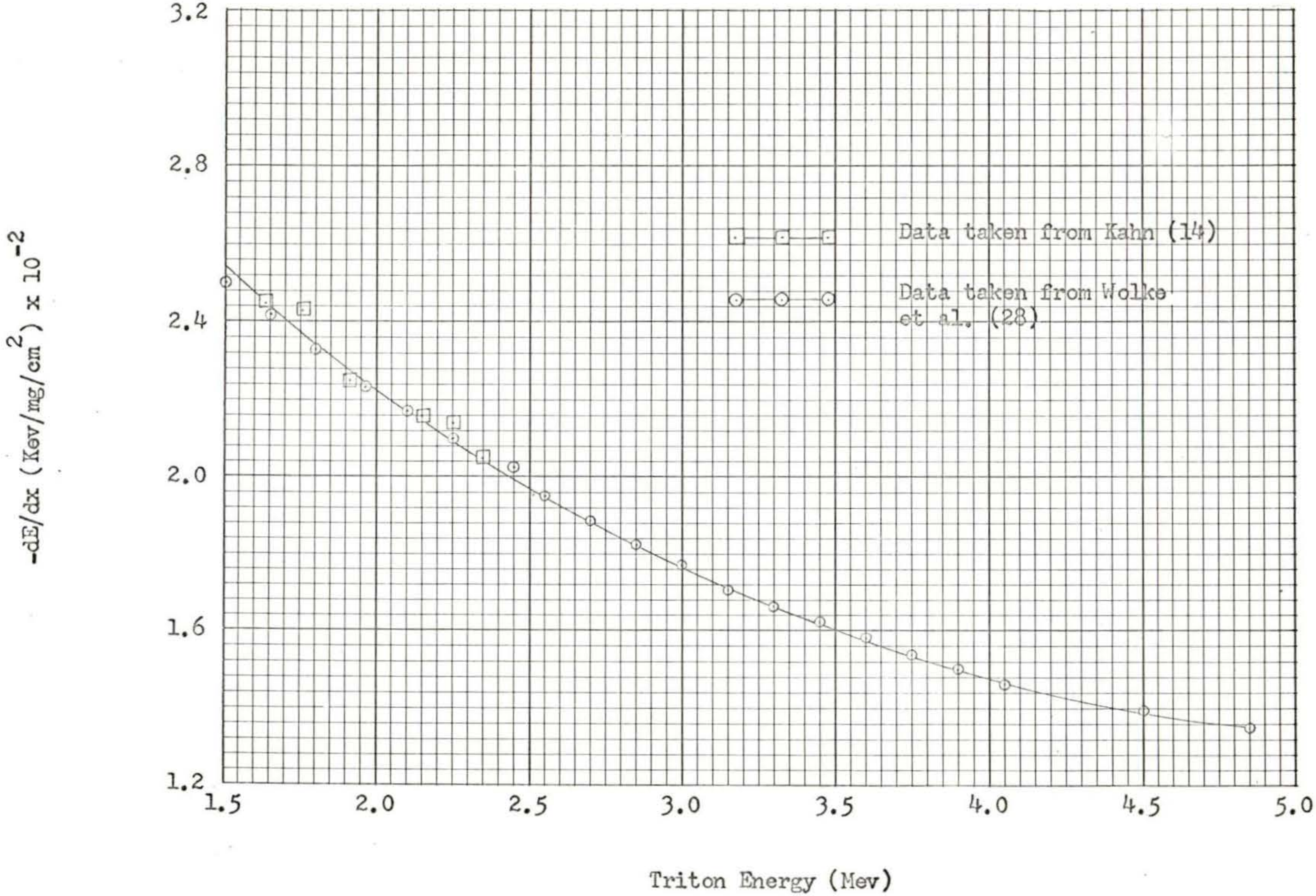

Figure 11. Specific energy loss of tritons (in aluminum) vs triton energy

to entering and just after leaving the "catcher" foil.

4. b was found by extrapolating this line to zero triton energy.

5. E_T' was taken to be the mean energy of the triton during its passage through the "catcher" foil.

The results of energy loss calculations in the air and in the "catcher" foil are shown in Table 3.

Detection System Efficiency

Calculations of the efficiency of this detection system for detection of neutrons of chosen energy are based on data presented by Goldberg et al. (13). This volume presents differential scattering cross section data as a function of triton scattering angle in the center-of-mass system at various neutron energies. Figure 12 shows a sample plot of this data for neutron energy of 0.30 Mev. Similar curves are given by Goldberg et al. (13) for neutron energies of 0.15, 0.20, 0.258, 0.27, 0.35, 0.40, 0.565, 0.60, 1.10, 1.5, 2.0, and 2.15 Mev. The data presented for each value of neutron energy is normalized to correspond to the cross section vs neutron energy curve shown in Figure 6. Thus, the cross section for triton scattering into a solid angle of 4π steradians for a given neutron energy is just the value of cross section found in Figure 6 for that same neutron energy. By graphical integration of curves such as Figure 12, it is possible, knowing the triton scattering angle, to calculate the effective cross section for triton scattering into any given angle.

Table 3. Triton energy loss calculations

Neutron Energy (Mev)	Triton Energy (Mev)	$\frac{dE}{dx}$ (air) (Kev/mg/cm^2)	Energy loss in 0.186 mg/cm^2 of air (Mev)	Energy loss in 4.83 mg/cm^2 of Aluminum (Mev)	$\frac{dE}{dx}$ (air) (Kev/mg/cm^2)	Energy loss in 0.23 mg/cm^2 of air (Mev)	Triton Energy (Mev)
Thermals	2.730	246	0.0460	1.020	332	0.0764	1.588
0.150	3.055	231	0.0430	0.955	300	0.0690	1.988
0.200	3.112	228	0.0424	0.940	296	0.0680	2.062
0.258	3.180	225	0.0418	0.913	282	0.0650	2.160
0.270	3.200	224	0.0416	0.910	280	0.0645	2.184
0.300	3.232	222	0.0413	0.906	278	0.0640	2.221
0.350	3.289	221	0.0411	0.892	270	0.0620	2.289
0.400	3.345	219	0.0407	0.879	266	0.0610	2.369
0.565	3.506	212	0.0394	0.846	252	0.0580	2.562
0.600	3.550	210	0.0390	0.840	251	0.0576	2.609
1.100	4.012	193	0.0359	0.770	228	0.0525	3.142
1.500	4.370	180	0.0335	0.723	210	0.0483	3.565
2.000	4.795	170	0.0316	0.684	193	0.0444	4.035
2.150	4.930	169	0.0314	0.680	188	0.0433	4.167
Thermals No Al	2.730	246	0.1020 *				

* thickness of air = 0.416 mg/cm^2

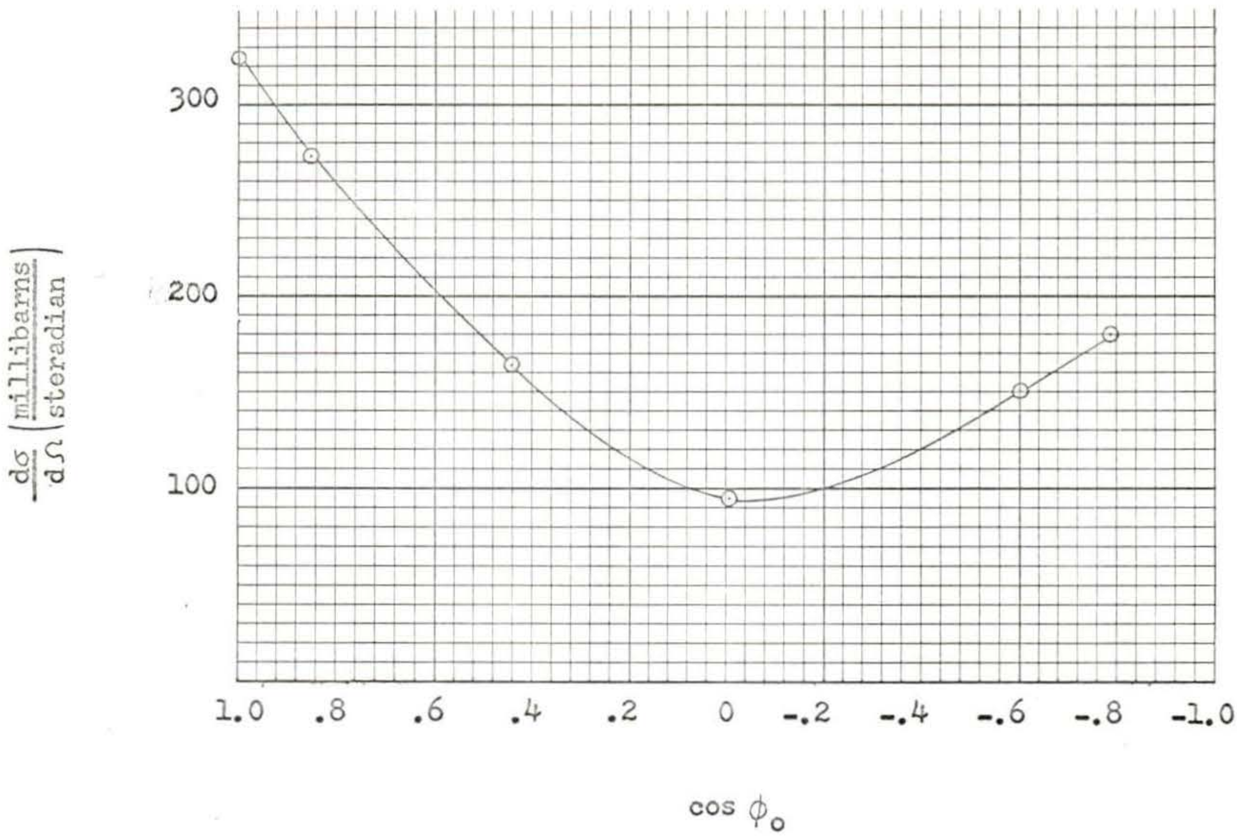

Figure 12. Differential scattering cross section for tritons from the $Li^6(n,T)He^4$ reaction. Neutron energy is 0.30 Mev.

For this system, the triton scattering angle in the laboratory system was taken to be 18.4 degrees. This represents the case where the neutron reaction in the Li^6F foil takes place on the axis of one of the grid holes and the resulting triton is scattered at an angle of 18.4 degrees from this axis. This is the largest angle at which the triton can be scattered from the selected point and still be detected by the detector (see Figure 8). The corresponding angle in the center-of-mass system can be calculated using Equation 19. It is seen that this angle (in the center-of-mass system) is dependent on the energy of the incident neutron.

If the cross section for triton scattering into the allowed scattering angle is known, the fraction f(E) of incident neutrons of a given energy which produce tritons that are detected can be calculated from the following equation,

$$f(E) = N\,dx\ \sigma(\phi_o) \tag{23}$$

where N is the number of Li^6 atoms/cm^3 in the Li^6F foil, dx is the linear thickness of the Li^6F foil, and $\sigma(\phi_o)$ is the effective cross section determined above. For the Li^6F foil used in this work, N and dx were calculated to be 6.26×10^{22} atoms/cm^3 and 5.96×10^{-5} cm respectively.

Table 4 lists values of ϕ_o, $\sigma(\phi_o)$, and f(E) as calculated for the neutron energies of interest in this work.

It should be noted that the efficiencies calculated as discussed above are only relative efficiencies. Neutrons incident on the Li^6F foil at angles other than 90° will travel a greater distance in the foil and thus have a greater probability of interacting with Li^6 and yielding a detectable triton. Since the fission neutrons are emitted from the fission plate isotropically, the relative number of neutrons incident on the Li^6F foil at any given angle will be the same for all neutron energies.

Since relative efficiencies provide the desired information, absolute detection system efficiencies have not been calculated.

Table 4. Relative detection system efficiency

Neutron Energy (Mev)	ϕ_o (degrees)	$\sigma(\phi_o)$ (millibarns)	f(E) (x 10^7)
0.15	19.90	055.8	2.080
0.20	20.00	124.0	4.620
0.258	20.20	184.0	6.850
0.270	20.25	170.0	6.350
0.300	20.35	132.0	4.910
0.350	20.50	083.8	3.130
0.400	20.70	084.6	3.160
0.565	20.95	027.2	1.015
0.600	21.00	028.8	1.072
1.100	21.50	029.0	1.084
1.500	21.90	025.2	0.940
2.000	22.25	014.9	0.555
2.150	22.40	012.1	0.491

Energy Resolution

The energy resolution of this detection system is dependent on five separate factors. These are:

a. Electronic noise in the detector, preamplifier, amplifier, and analyzer system.

b. Variations in triton energy losses in the Li^6F foil.

c. Variations in triton energy losses in air and in the aluminum "catcher" foil.

d. The background contribution from such other sources as gamma rays.

e. Variations in triton energies permitted by the geometry of the detection system.

The effect of the first four factors on the total resolution of the system can be determined experimentally while the effect of the system geometry must be accounted for analytically.

Calibration of the detection system

Prior to the experimental determination of the effect of the above listed factors on the total resolution of the system, the energy calibration of the detection system was performed. That is, the channel in which the pulse produced by a given energy particle will be stored, was determined. The energy width of each channel was also found.

The detection system used in this work was calibrated using a source of monoenergetic alpha-particles, (Am^{241} , $E_{\alpha} = 5.477$ Mev) and a voltage pulse generator. A schematic drawing of the circuit used is shown in Figure 13.

The output of the pulse generator was fed through a one picofarad capacitor (inside the preamplifier housing) to the preamplifier. The generator pulses are passed through the preamplifier and linear amplifier at the same time as pulses from the detector. Calibration consists of detecting alpha particles of known energy with the detector and simultaneously adjusting the amplitude of the pulses from the pulse generator until the respective spectrum peaks fall in the same channel of the

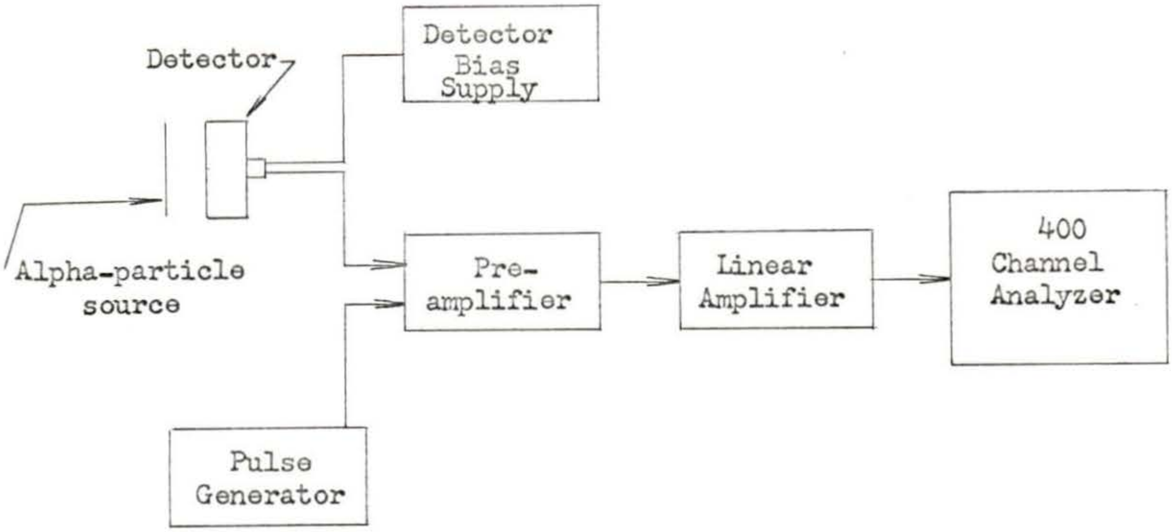

Figure 13. Schematic of circuit used to calibrate the detection system

analyzer. Controls on the pulse generator permit the pulser output to be normalized to the alpha particle energy, i.e., the pulser settings can be adjusted so that the alpha particle energy is set directly on the dial of the pulse generator. Thus, any other particle energy can be read from the dial settings when the pulse generator output is adjusted to fall in the same channel as the pulse from the particle. This absolute calibration makes detailed knowledge of circuit gain, etc. unnecessary.

The width of each channel was determined by observing the output of the pulse generator at two different settings (each setting corresponding to a given energy particle). The equivalent energy difference between the two pulser settings divided by the number of channels between the resulting peaks yielded the channel width. As adjusted for these experiments, the multichannel analyzer channel width was found to be 8.9 Kev.

Effect of electronic noise on total system resolution

The contribution to the total resolution of the system due to electronic noise was determined by observing the full width at half maximum of a peak produced by the pulse generator. The circuit shown in Figure 13 was used. A plot of this data is shown in Figure 14 where the FWHM is seen to be 52 Kev. The output of the pulse generator when fed directly into the linear amplifier (preamplifier, detector, and power supply not included in the circuit) yielded an essentially "one-channel" profile.

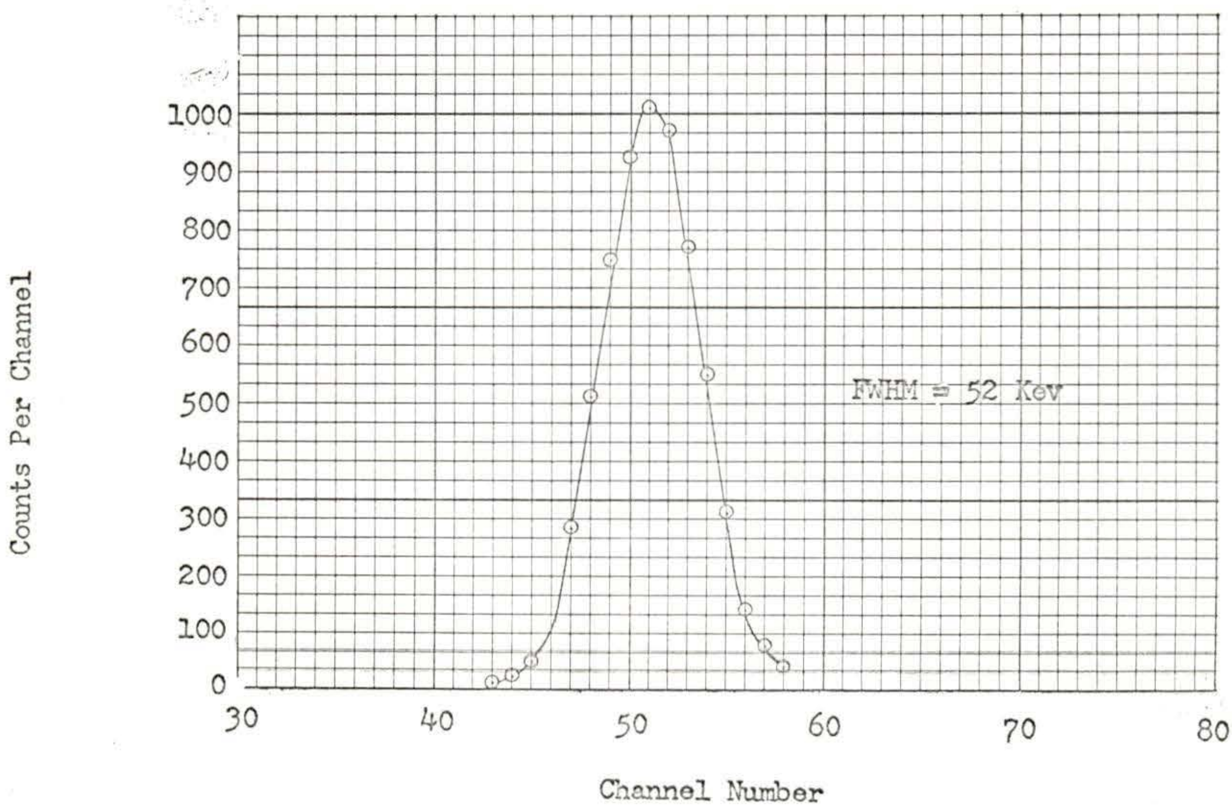

Figure 14. Energy resolution of pulse generator output (see Appendix C, Table 7 for data)

Effect of triton energy losses in Li^6F foil on total system resolution

The effect on the energy resolution of triton energy losses in the Li^6F foil was determined by counting only thermal neutrons and observing the FWHM of the resulting triton peak. The same detector geometry as seen in Figure 7 was maintained here with the exception that no aluminum "catcher" foil was in place. In the absence of the "catcher" foil, both tritons and alpha particles were detected. The energy of the particles, i.e., 2.73 Mev for tritons and 2.05 Mev for alpha particles caused the respective peaks to be separated and thus permitted the analysis of the triton peak. The triton peak is plotted on Figure 15 and the FWHM was found to be 75 Kev.

Effect of triton energy loss variations in the "catcher" foil on the total system resolution

This effect was determined by putting the aluminum "catcher" foil in place and again observing the FWHM of the triton peak produced by detecting only thermal neutrons. This data is plotted on Figure 16 and the FWHM was found to be 148 Kev. It is noted that the value of FWHM shown in Figure 16 includes the contribution due to electronic noise and energy losses in the Li^6F foil as well as that due to energy loss variations in the "catcher" foil. In the subsequent analysis, the resultant effect of the above three resolution factors will be considered as a single contribution to the total resolution of this detection system. It is assumed that this contribution is constant for the neutron energies of interest in this work.

The contribution from gamma radiation, if large enough, will render the derived distribution statistically meaningless.

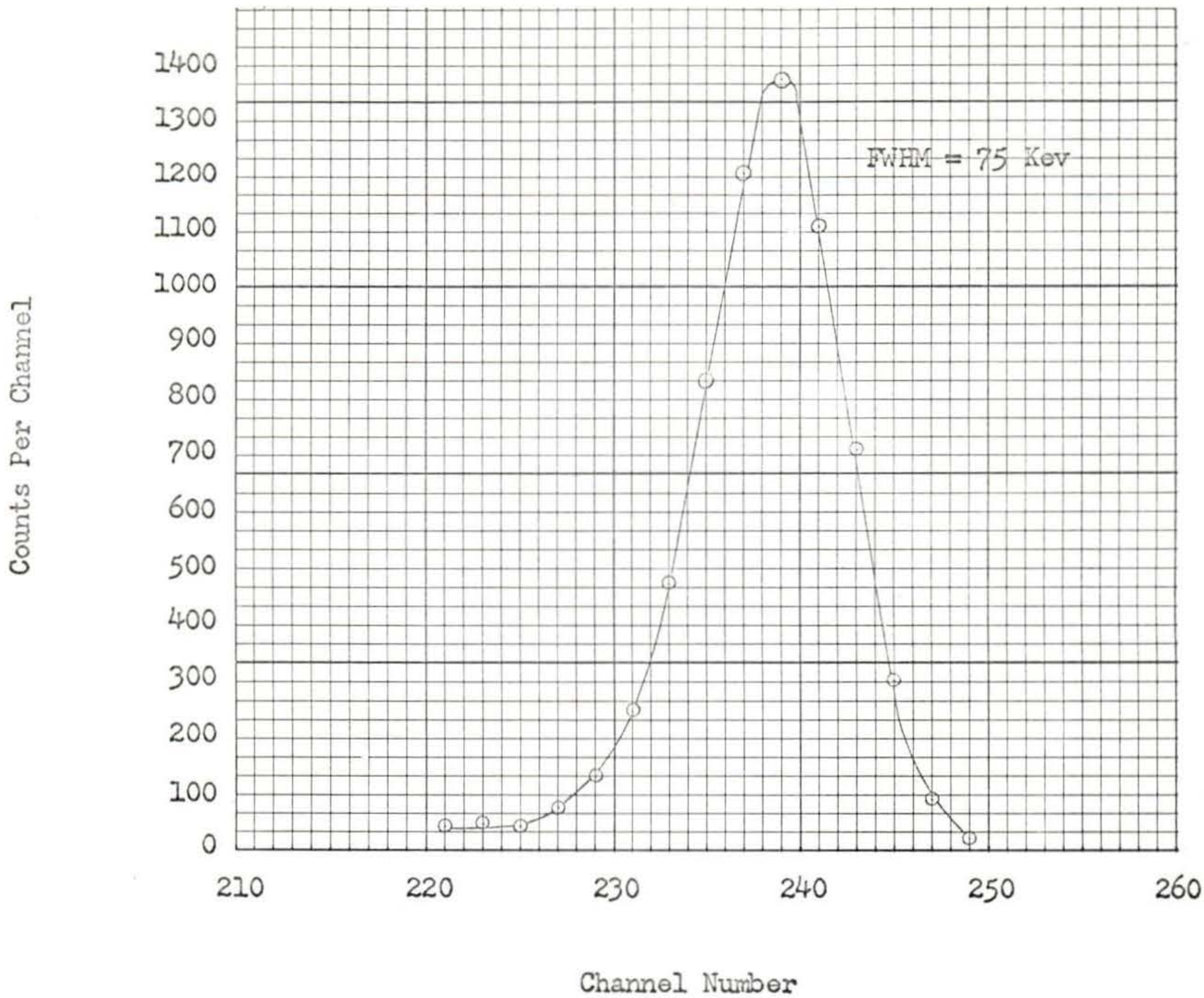

Figure 15. Energy resolution of triton peak produced by thermal neutrons (see Appendix C, Table 8 for data)

Contribution to total system resolution of system geometry

As can be seen from Equation 21, the energy of the triton resulting from the $Li^6(n,T)He^4$ reaction is dependent on the neutron energy and the angle (in the center-of-mass system) at which the triton is scattered with respect to the direction of travel of the incident neutron. For neutrons of a given energy, the triton energy will range from the value calculated when $\phi_o = 0^\circ$, to that calculated when ϕ_o is the maximum as

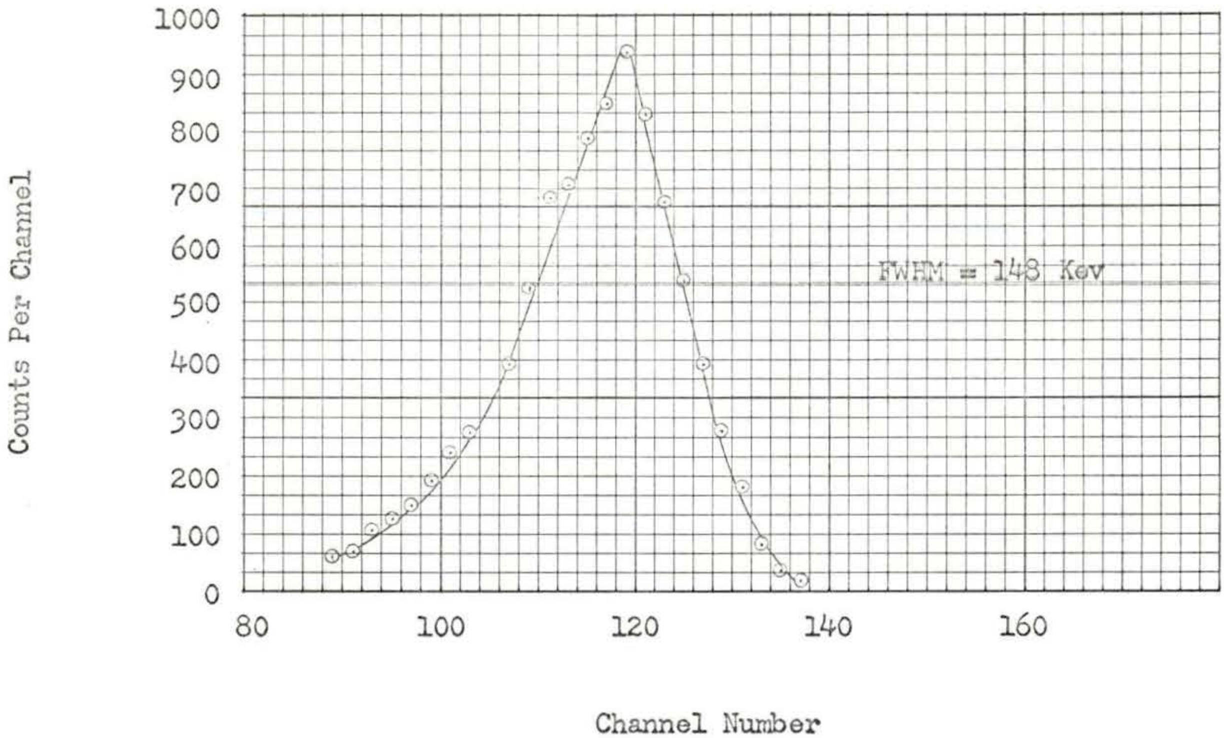

Figure 16. Energy resolution of triton peak produced by thermal neutrons with "catcher" foil in place (see Appendix C, Table 9 for data)

allowed by the detection system geometry. To permit a determination of the effect of this variation in triton energy on the FWHM of a triton peak at any given neutron energy, it was assumed that the distribution of triton energies for monoenergetic neutrons would have a shape similar to the normal (Gaussian) distribution. From Price (26, p. 58) the FWHM is then $2.36\,\omega$ where ω is the standard deviation of the pulse height distribution or, in this case, the triton energy distribution. From the characteristics of the normal distribution function, ω is here taken to be 1/6 of the total triton energy spread, ΔE_T. Table 5 shows the FWHM determined by this method for each of the chosen values of neutron energy.

Total resolution of detection system

The total resolution (FWHM) of this detection system is thus the sum of the two "partial" widths determined above. If there is no correlation between the uncertainties in the determination of neutron energy for the individual "partial" widths, and if each has a Gaussian distribution in amplitude, the total width (FWHM) can be determined by the following quadratic form,

$$\delta = \sqrt{\sum \delta_i^2} \qquad (24)$$

where δ is the total system resolution and δ_i represents the i "partial" widths.

Rybakov and Sidorov (27), in their treatment of this subject, note that this method of combining partial widths does not introduce any significant error even when the distribution of uncertainties is not Gaussian.

The total resolution of this detection system excluding background for each value of neutron energy is shown in Table 6. Results are included for the system with and without the "catcher" foil.

Figure 17 shows a plot of the total system resolution as a function of neutron energy.

Table 5. System geometry contribution to total resolution

Neutron Energy (Mev)	$(\phi_o)_{min}$ (degrees)	$(\phi_o)_{max}$ (degrees)	$(E_T)_{min}$ (Mev)	$(E_T)_{max}$ (Mev)	ΔE_T (Mev)	FWHM (Mev)
0.150	0	57.90	3.000	3.110	0.110	0.043
0.200	0	58.10	3.041	3.194	0.153	0.060
0.258	0	58.25	3.100	3.270	0.170	0.067
0.270	0	58.30	3.110	3.290	0.180	0.070
0.300	0	58.50	3.140	3.335	0.195	0.076
0.350	0	58.80	3.182	3.396	0.214	0.084
0.400	0	59.25	3.230	3.460	0.230	0.090
0.565	0	60.00	3.362	3.650	0.288	0.113
0.600	0	60.25	3.400	3.700	0.300	0.118
1.100	0	61.60	3.784	4.240	0.456	0.179
1.500	0	62.50	4.080	4.660	0.580	0.228
2.000	0	63.50	4.440	5.150	0.710	0.279
2.150	0	63.90	4.560	5.300	0.740	0.291

Table 6. Total energy resolution of detection system with and without the aluminum "catcher" foil

Neutron Energy (Mev)	Total Resolution with foil (FWHM) (Mev)	% Resolution	Total Resolution with no foil (FWHM) (Kev)	% Resolution
0.150	0.154	103	86	57
0.200	0.159	79	96	48
0.258	0.163	63	100	39
0.270	0.164	61	103	38
0.300	0.167	56	107	36
0.350	0.170	49	112	32
0.400	0.174	43	117	29
0.565	0.186	33	135	24
0.600	0.189	31	139	23
1.100	0.232	21	194	18
1.500	0.272	18	240	16
2.000	0.316	16	289	15
2.150	0.327	15	300	14

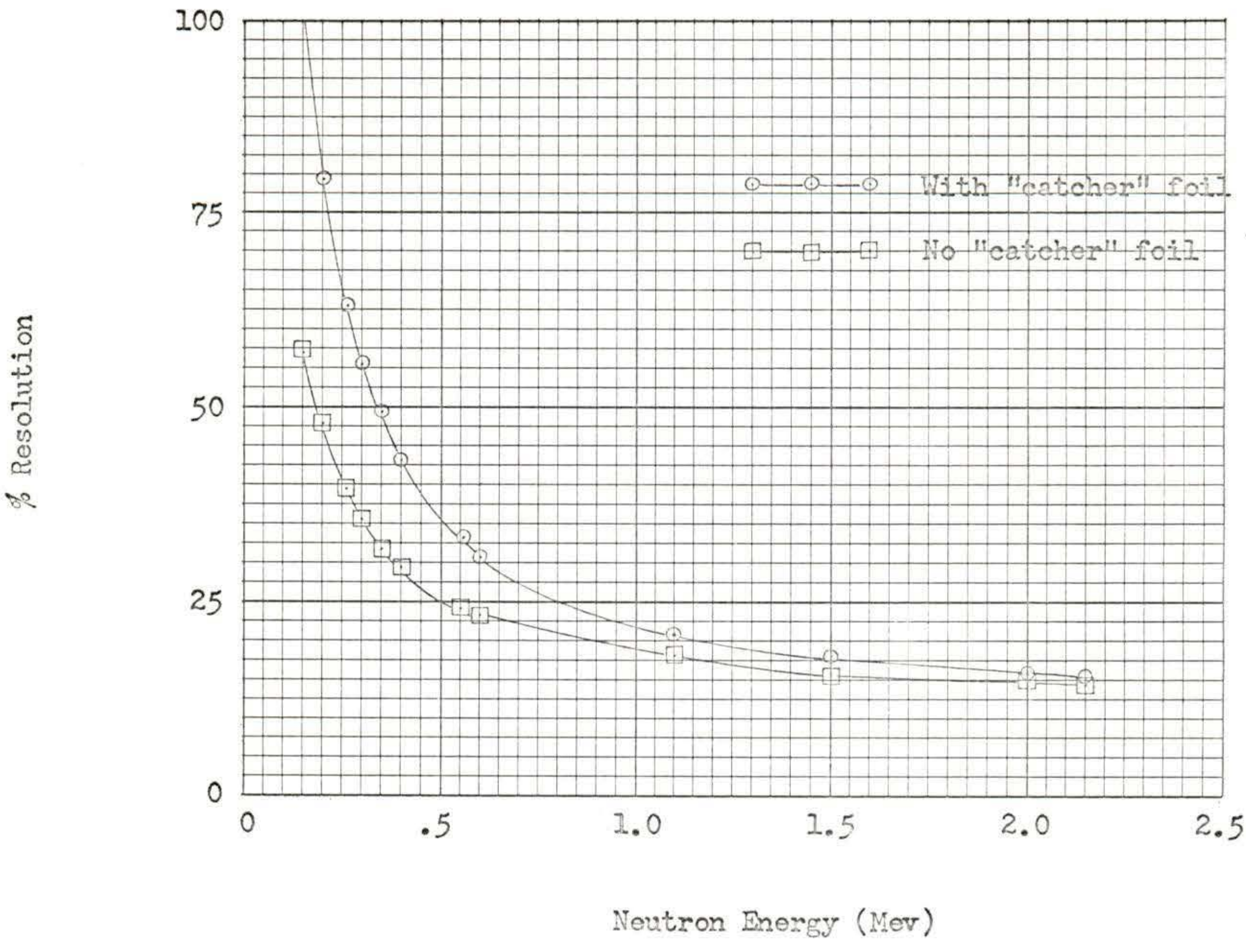

Figure 17. Total detection system resolution vs neutron energy

EXPERIMENTAL EQUIPMENT AND PROCEDURE

The experimental equipment incorporated into this detection system was selected in an effort to develop a low cost neutron spectrometer requiring a minimum of electronic apparatus and yet having satisfactory resolution and efficiency characteristics as compared to other methods. The system under discussion, utilizing a single semiconductor detector, satisfies these requirements.

The principle disadvantage of a system of this type is that all effects of gamma rays and charged-particle reactions other than the $Li^6(n,T)He^4$ reaction must be eliminated either by shielding the detector (in the case of gamma rays) or by doing background runs. In the coincidence systems, for example, these effects are eliminated electronically. The cost of the coincidence type spectrometer system, however, is a significant consideration.

The principle experimental objective was to demonstrate the ability of the proposed detection system to resolve the fission spectrum of U-235 in the energy range from 0.15 to 2.15 Mev. Determination of the effects produced by gamma rays and fast neutron induced charged-particle reaction was also of prime significance.

The source of fast neutrons was a fission foil of uranium 93% enriched in U-235. The energy spectrum of prompt neutrons released as a result of thermal fission of U-235 is well known and is given, for example, in Etherington (8, p. 7-91).

Calibration of the detection system and experimental determination of the various resolution effects have been described in the section on detection system analysis and are not repeated here.

The apparatus which was used for the initial experimental runs is shown in Figure 18.

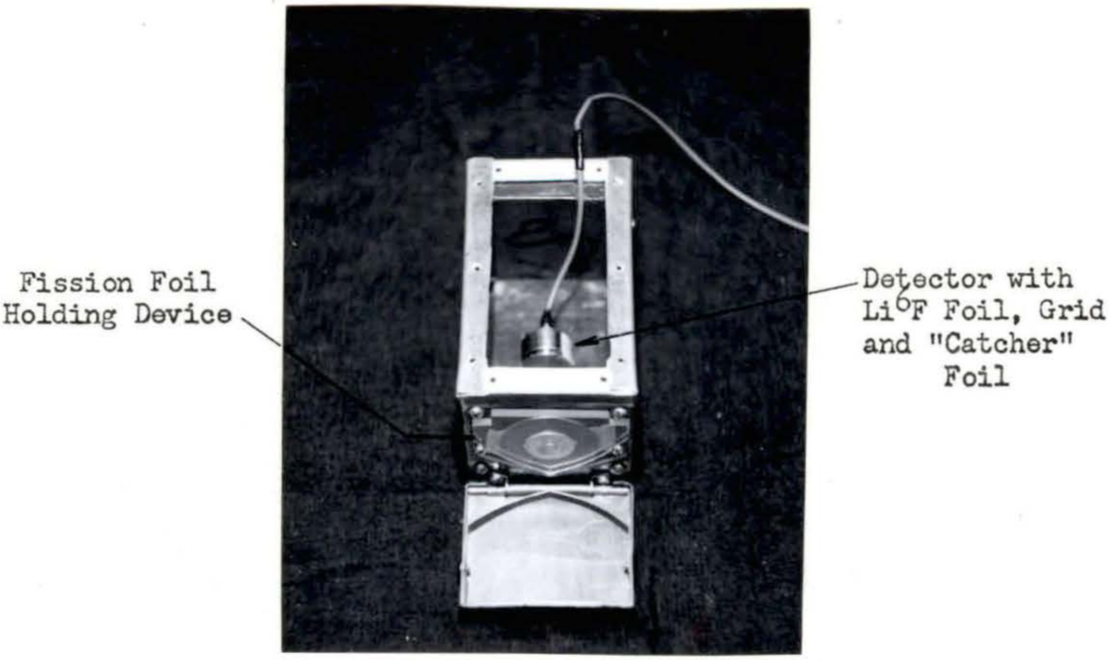

Figure 18. Apparatus for initial runs inside thermal column

The box, constructed of 0.031 inch sheet aluminum, provided fixed system geometry. To reduce the thermal neutron flux at the location of the "converter" foil and detector, the box was covered with 0.030 inch cadmium, excepting a 1 inch diameter hole of the location of the fission foils.

Prior to doing experimental work with the detection system in the reactor, two reactor runs were made to determine reactivity effects introduced by placing fission foils in the thermal column of the UTR-10. An initial run was made with the cadmium covered box (no fission foils) placed in the opening normally occupied by the central stringer of the thermal column at a distance of 26 inches from the "south" core tank. The location of the box relative to the core is shown in Figure 19.

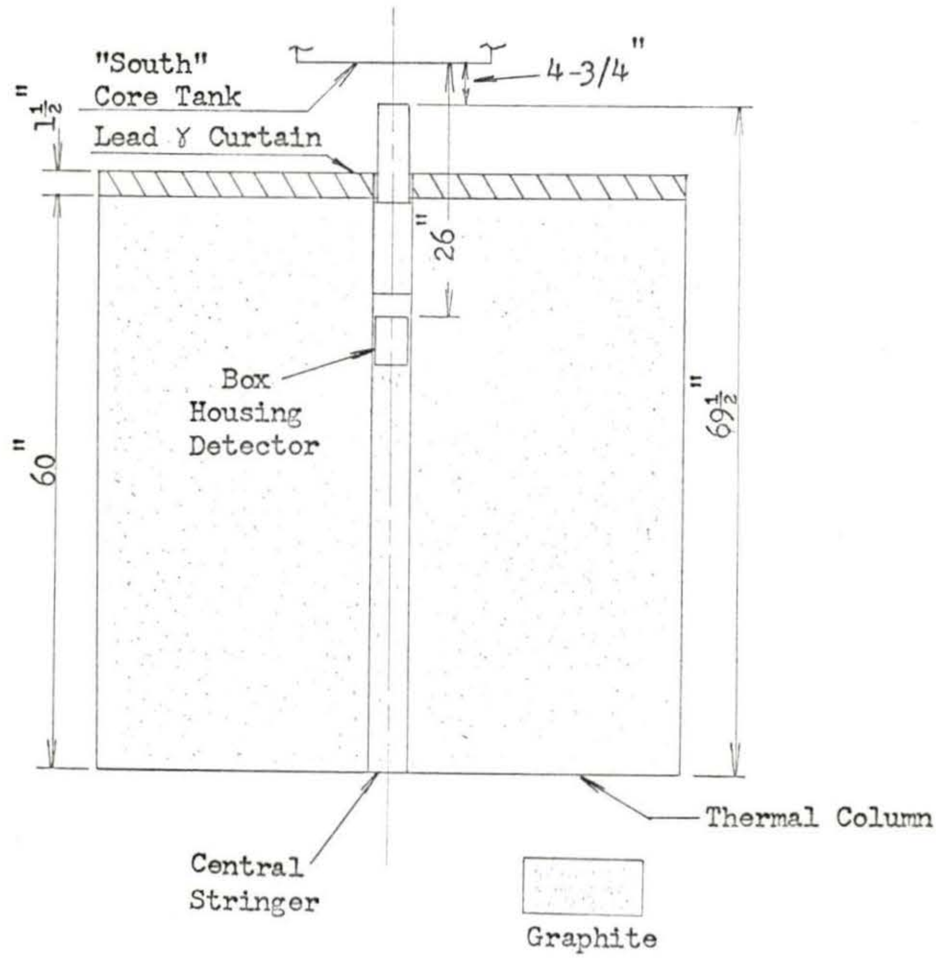

Figure 19. Relative location of UTR-10 thermal column and "south" core tank

The control rod positions and moderator inlet and outlet temperatures were recorded with the reactor power level at 1 watt. A subsequent run was made under identical conditions as during the first run except that two fission foils were attached to the front of the cadmium covered box. At the same power level of 1 watt, it was found that all control rod position readings and moderator temperature readings were the same as for the previous run, indicating that the fission foils (10 grams total mass) had a negligible effect on the reactivity of the UTR-10 reactor.

Investigation of System Operation Inside the Thermal Column

The initial experimental run in the thermal column was made using the apparatus shown in Figure 18. The fission plate, "converter" foil, grid with "catcher" foil, and detector were positioned as shown in Figure 7. The detector was covered with 0.030 inch cadmium. The box was placed in the opening normally occupied by the central stringer of the thermal column at a point 32 inches from the "south" core tank. That portion of the opening between the box and the core tank was filled with graphite. With the reactor power level at 300 watts, data was taken for a 10 minute period. A plot of the results is shown in Figure 20.

It is seen that the triton peak from thermal neutron reactions in the "converter" foil is located in channel number 71 (i.e. 1.80 Mev). From the triton energy loss calculations and the calibration data, this peak was expected to fall in or slightly below channel number 45. The resolution of this triton peak was also much worse than had been expected.

These results could be explained if the neutron flux at the detector location included a significant high energy component. That is,

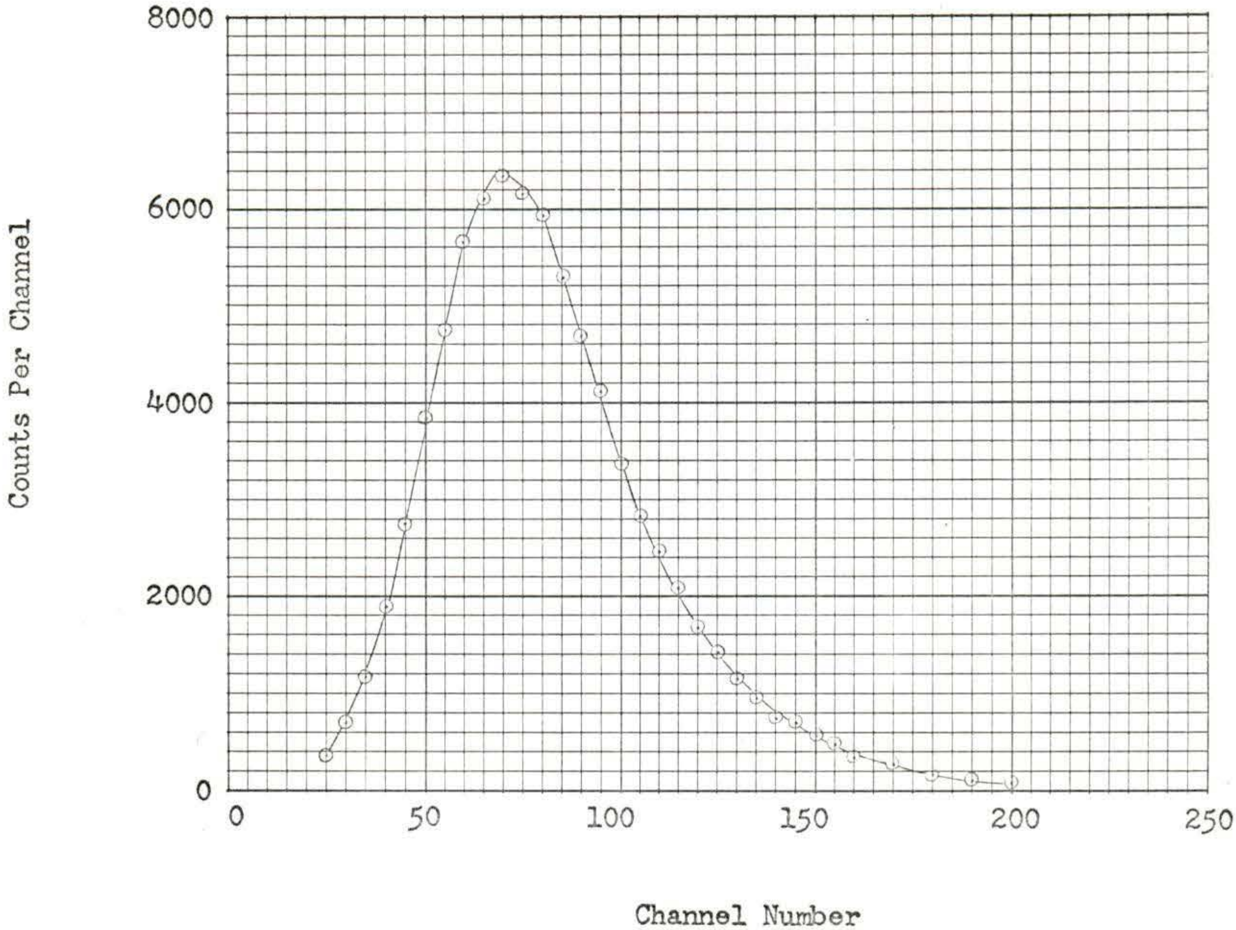

Figure 20. Plot of results obtained with detection system inside thermal column at point 32 inches from "south" core tank (see Appendix C, Table 10 for data)

a significant fraction of the neutrons at this point in the thermal column had not yet been completely thermalized and the detector was indicating this.

The apparatus was then modified as shown in Figure 21. The alternating layers of 0.125 inch plexiglas and 0.030 inch cadmium were intended to moderate and then capture epi-cadmium neutrons that passed through the cadmium surrounding the aluminum box. The apparatus was

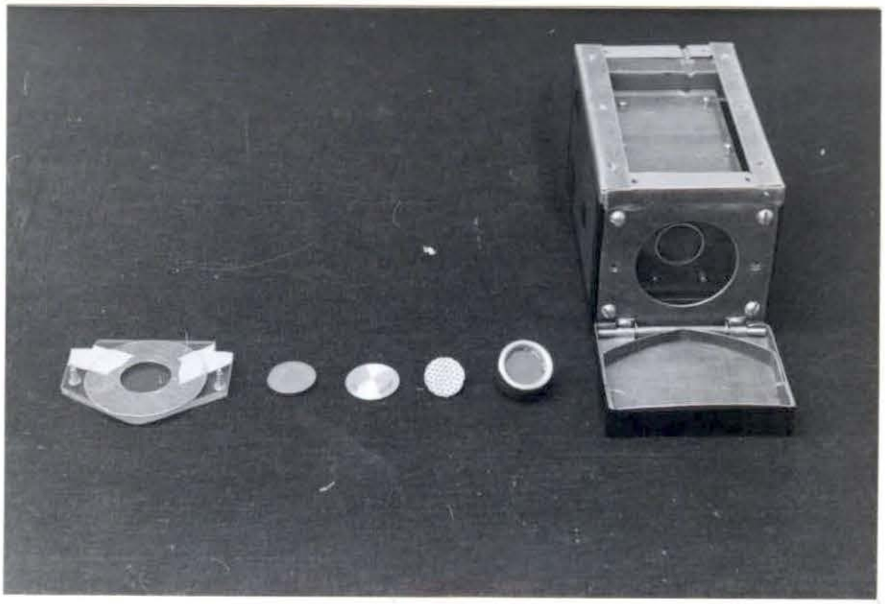

Figure 21. Modification of apparatus incorporating two alternating layers of plexiglas and cadmium. Items from left to right include the fission foil holding device, fission foil, Li^6F "converter" foil, grid with "catcher" foil, detector, and cadmium covered box with modification.

positioned 46 inches from the core tank, i.e. (withdrawn a further 14 inches into the thermal column), to determine if the assumption of incomplete thermalization could explain the results found previously. Using one fission foil, data was taken for 15 minutes at a reactor power level of 600 watts. The results obtained were very similar to those obtained previously, i.e. the peak was located in channel number 72 and no improvement in resolution was noted. An additional run was then made without fission foils. Counting was done for 8 minutes at a power level of 600 watts. No improvement in peak location or resolution was found.

The apparatus was then relocated at the end of the thermal column where effects due to incomplete thermalization would be minimized and data taken.

Since a fraction of the incident thermal neutrons will pass through the fission foils and reach the converter, it is necessary to subtract such contributions to obtain a meaningful fission spectrum measurement. A foil of lead and cadmium having the same thermal neutron absorbing and scattering properties as the fission foils was made (for details see Appendix B). The thermal neutron contribution was eliminated by making identical runs using first the fission foils and then the lead-cadmium foil and identifying the difference as being due to fission neutrons.

Investigation of System Operation at the End of the Thermal Column

The apparatus was positioned with respect to the thermal column and and the thermal column door as shown in Figure 22.

To evaluate the resolution of the system in this new position, the reactor was brought to a power level of 5000 watts and the pulse generator

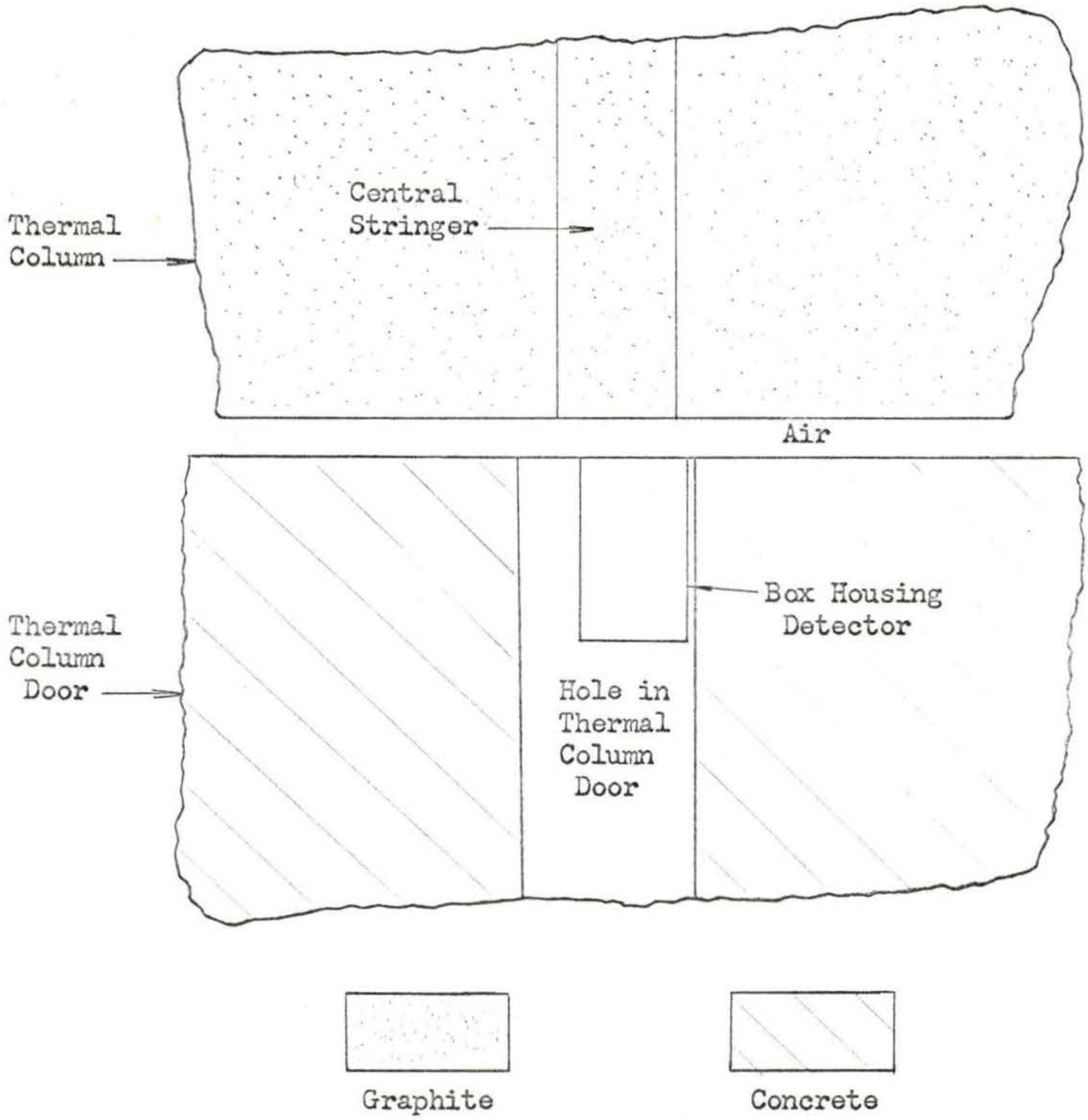

Figure 22. Position of apparatus for measurements at end of thermal column

was pulsed during the counting period. The FWHM of the peak obtained was nearly 3 times as great as that obtained when the reactor was at zero power. Figure 23 shows the results of this run. The pulse generator was then pulsed (120 pulses per second for 1.5 minutes) at

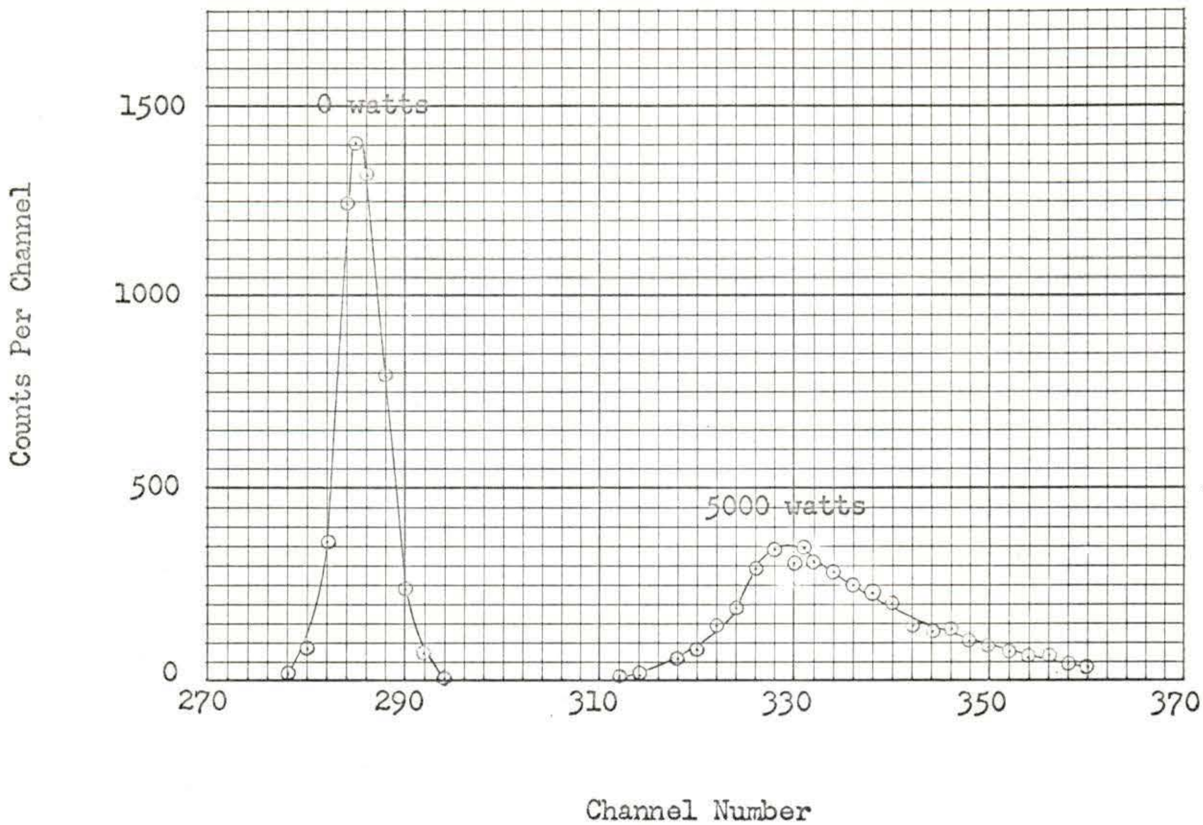

Figure 23. Resolution of pulse generator output at reactor power levels of 0 and 5000 watts (see Appendix C, Table 13 for data)

levels corresponding to 2.0, 2.5, 3.0, 3.5, and 4.04 Mev particle energy at reactor power levels of 0, 100, 500, 1000, and 2500 watts respectively. The peaks obtained from these runs are shown in Figure 24.

It was evident at this point that the location of the thermal triton peak and the poor resolution of this peak was due in part to gamma radiation rather than entirely to epi-cadmium neutrons. That is, the gamma rays incident on the detector were producing a strong background of small charge pulses. When a pulse from the detector or pulse generator was superimposed on this background, there was a certain probability of the

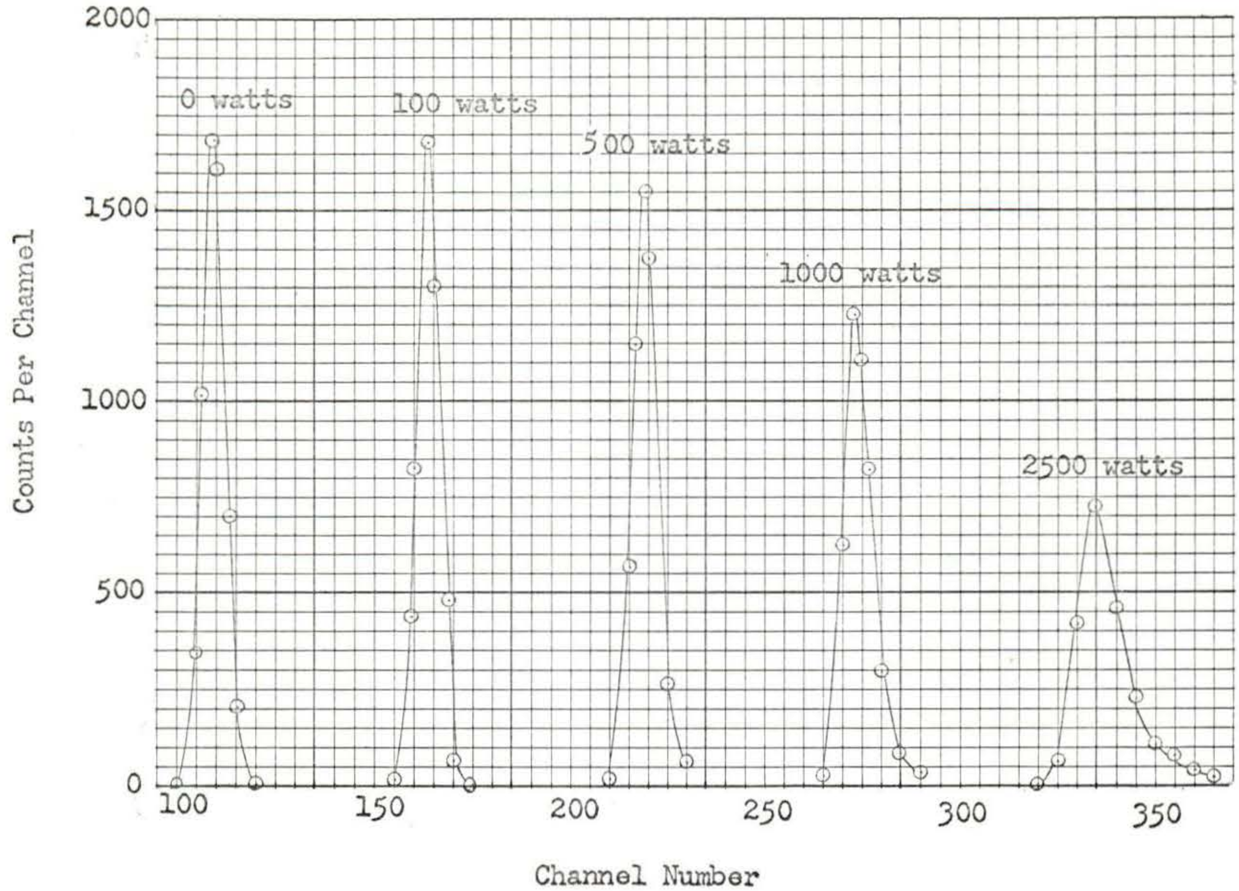

Figure 24. Resolution of pulser peaks at different reactor power levels with apparatus positioned as shown in Figure 22 (see Appendix C, Table 14 for data)

two pulses being produced at the same time. When this happened, the pulse from the detector or pulse generator appeared to be larger in magnitude than was expected. This variation in magnitude of the primary pulses was responsible for the resolution effects observed.

Subsequent runs were then made with the apparatus in the same position but shielded from gamma radiation from the core by a lead brick positioned as shown in Figure 25. The pulse generator was again pulsed (120 pulses per second for 1 min.) at levels corresponding to 2.08, 2.54, 3.08, and 3.50 Mev particle energy at reactor power levels of 0, 500, 1000, and 5000 watts respectively. The resulting peaks are shown in Figure 26. There was no significant change between the resolution obtained at corresponding power levels with and without the lead brick.

It was then postulated that the (n, γ) reaction in cadmium was responsible for the resolution effects. The absorption of a thermal neutron in cadmium occurs with the release of a gamma ray with energy in excess of 9 Mev. To eliminate this reaction, all the cadmium that had been used in the system was removed and boral (which produces an alpha particle) was substituted as the thermal neutron absorbing material. The boral used, in sheet form, was 0.125 inch total thickness of which 0.040 inches (0.020 inch cladding on each side) is aluminum. The center portion of the sandwich is a mixture of 35 weight per cent B_4C aluminum.

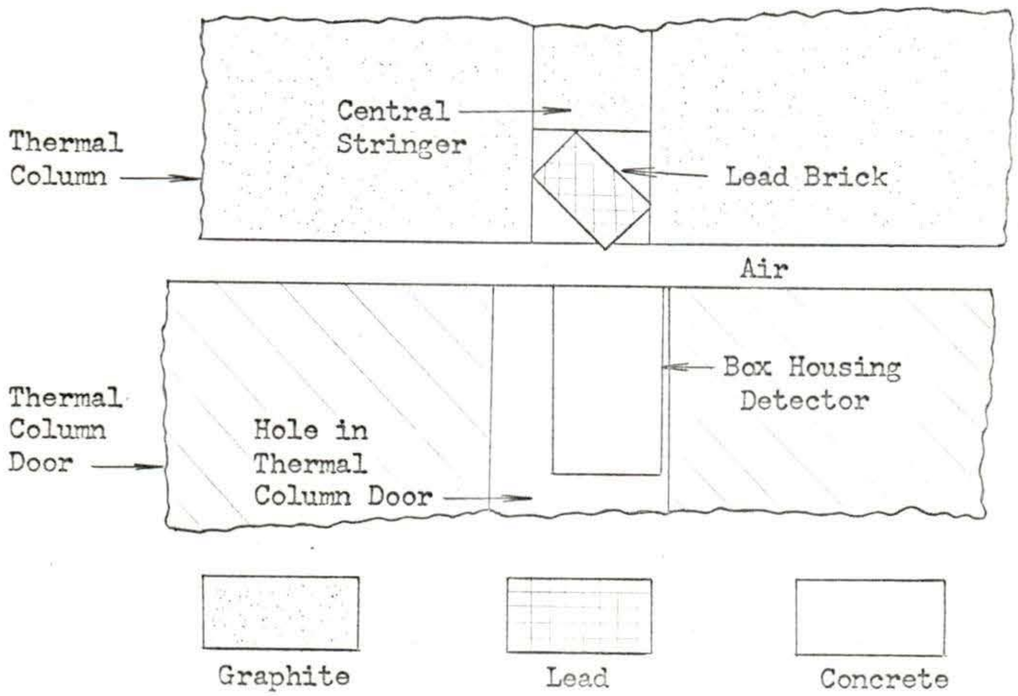

Figure 25. Position of lead shielding with apparatus at end of thermal column

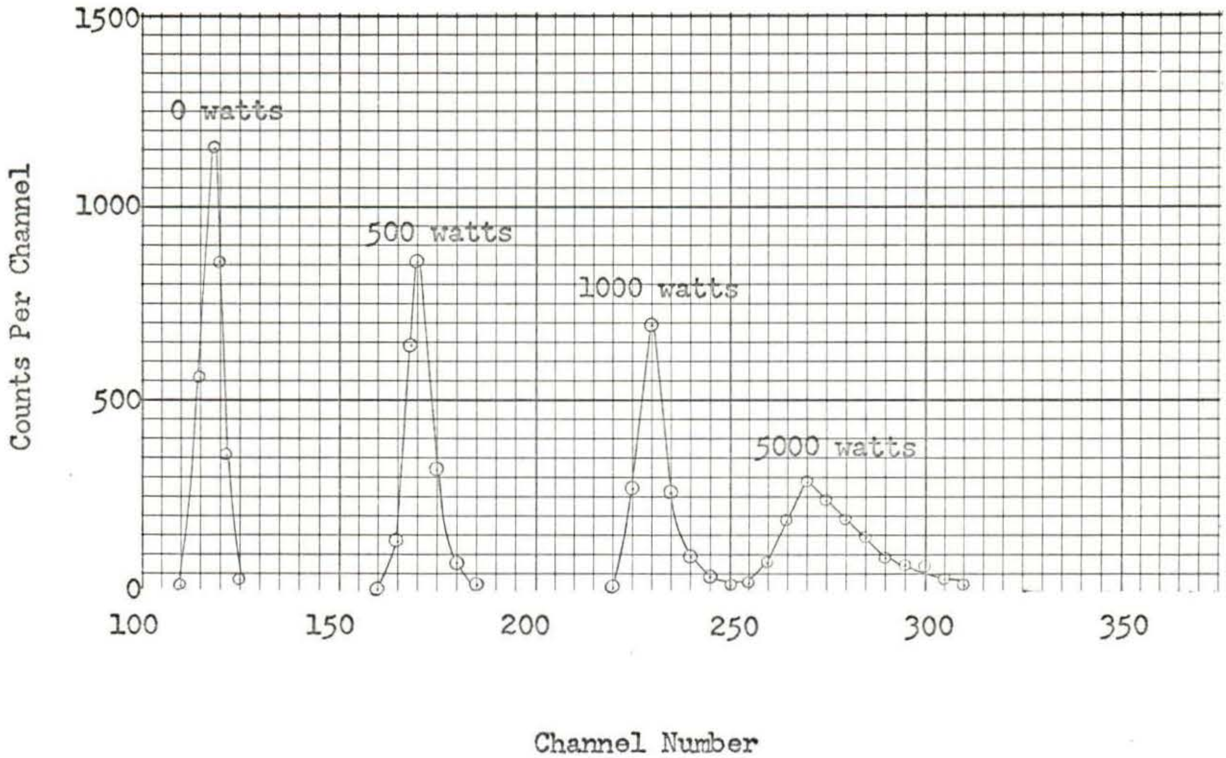

Figure 26. Resolution of pulser peaks at different reactor power levels with apparatus shielded as shown in Figure 25 (see Appendix C, Table 15 for data)

The first experimental run using boral was made with the apparatus as shown in Figure 27. The apparatus was positioned at the end of the thermal column as shown in Figure 25. The pulse generator was pulsed (120 pulses per second for 1 minute) at levels corresponding to 2.08, 2.54, 3.08, and 3.50 Mev particle energy at reactor power levels of 0, 500, 1000, and 5000 watts respectively. The resulting peaks are shown in Figure 28.

The peak resulting from detection of thermal neutrons at a reactor power level of 5000 watts is also plotted on Figure 28, and it is seen to fall where it was expected, i.e. channel number 51 for a threshold setting

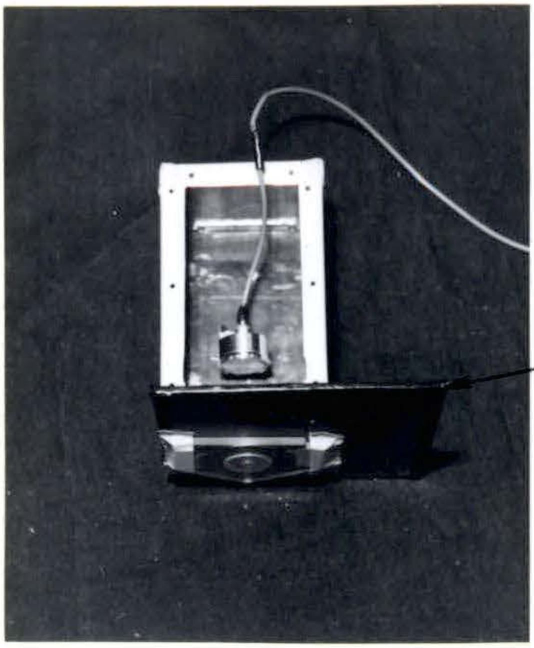

Boral Sheet,
1/8 inch thick

Figure 27. Apparatus with boral being used instead of cadmium

of 110.

Final modification of the apparatus consisted of adding additional boral and lead shielding. The apparatus then appeared as shown in Figure 29.

Three experimental runs were made to determine the ability of this detection system to resolve the fission spectrum in the energy range from .15 to 2.15 Mev. The first was made using 2 fission foils. The converter foil, grid and "catcher" foil were positioned as shown before. Data was

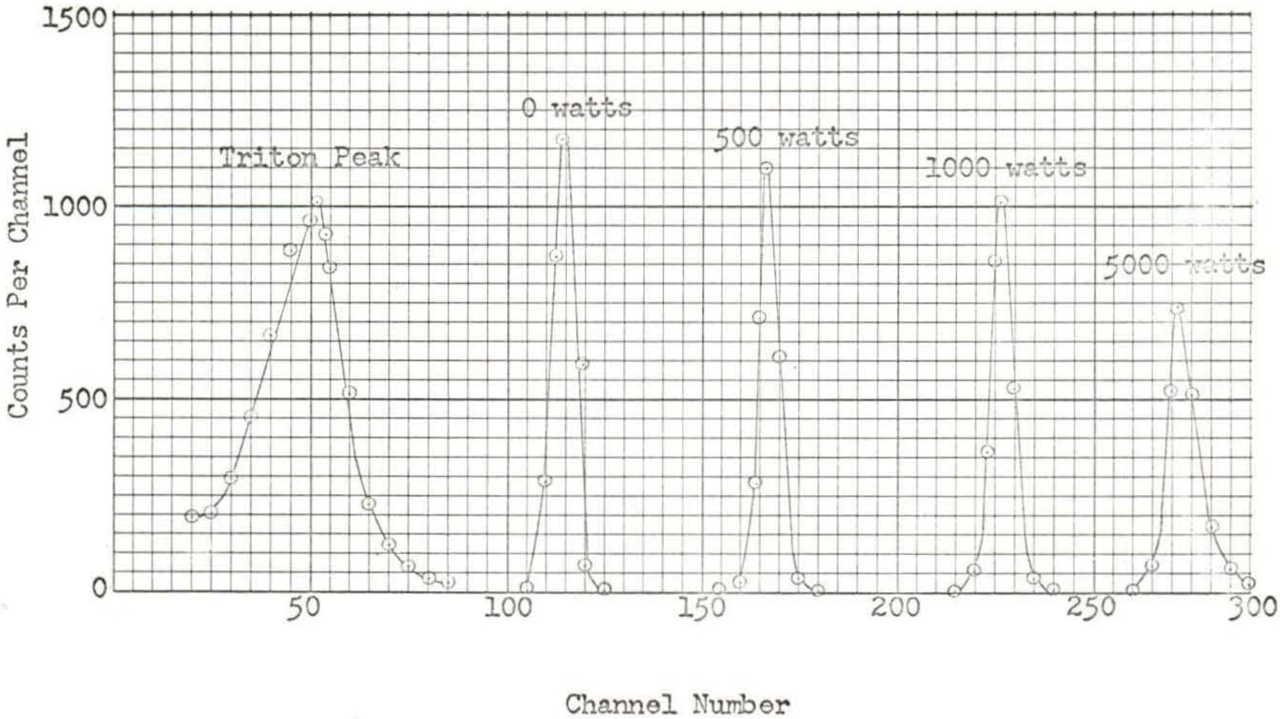

Figure 28. Resolution of pulser peaks with boral substituted for cadmium (see Appendix C, Table 16 for data)

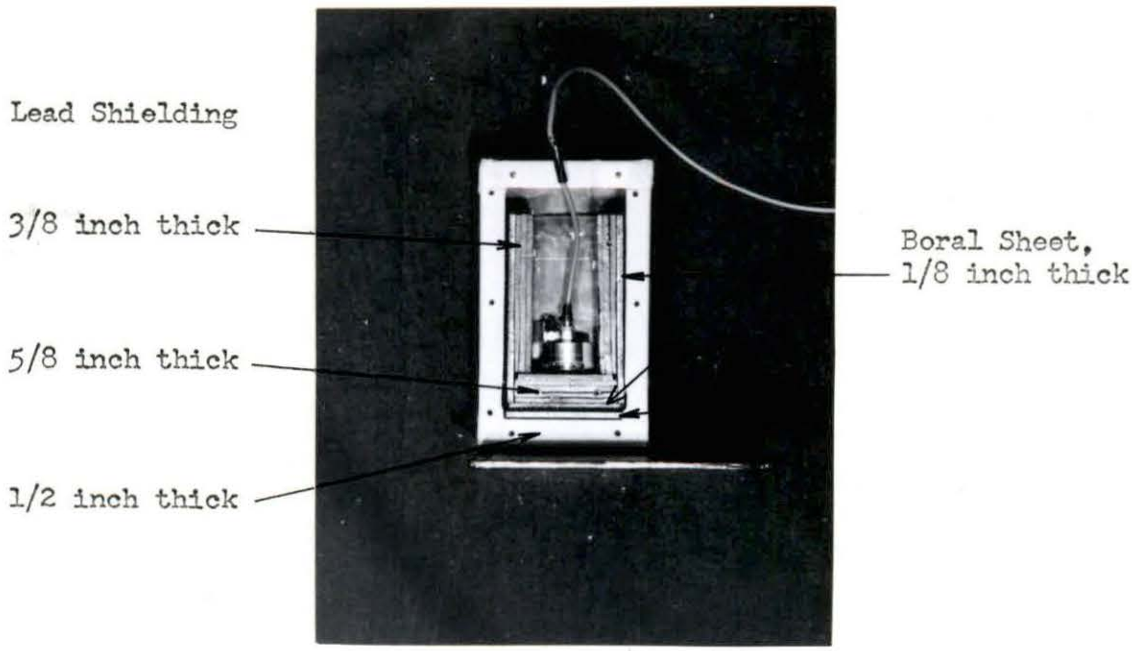

Figure 29. Detection system apparatus as used for final measurements

taken for 53 minutes at a reactor power level of 4000 watts. The second or background run was made with the lead-cadmium foil substituted for the fission foils. Data was again taken for 53 minutes at a power level of 4000 watts. The difference in the data from these two runs was due to the effects of the fission neutrons. The third run was made using 2 fission foils, however, the Li^6F "converter" foil was removed and replaced with an 18 mil foil of aluminum. The purpose of this run was to eliminate the counts due to both fast neutron reactions in the detector itself, and charged-particle reactions in the surrounding material. The information from this run indicated that the results of the two preceeding runs included a large component due to reactions other than those taking place in the Li^6F foil. Data obtained for the three runs is shown in Figure 30.

Subsequent investigation using a Po-Be neutron source (yielding neutrons with energies from approximately 2 to 10 Mev) indicated that fast neutron reactions in the detector itself were negligible compared to reactions involving the aluminum in the grid and "converter" foil. Apparently, in the presence of neutrons with energy above the threshold for the $Al^{27}(n,p)Mg^{27}$ reaction, the high background associated with the present design makes spectrum measurements difficult if not impossible.

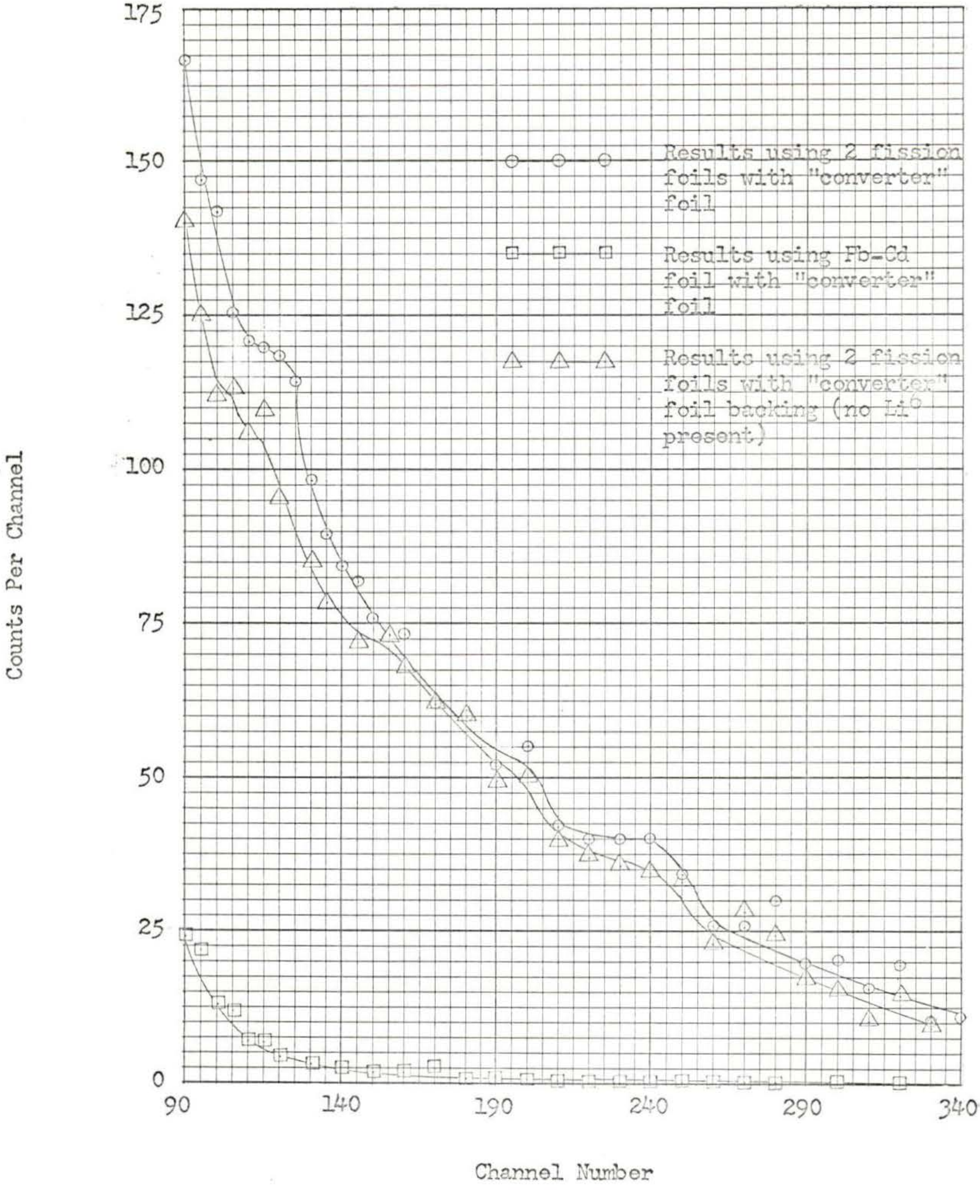

Figure 30. Results of final experimental runs (see Appendix C, Tables 17, 18, 19 for data)

RESULTS AND CONCLUSIONS

A detection system has been designed which, on the basis of the current analysis, appears suitable for measurement of neutron energies in the range from 0.15 to 2.15 Mev. This energy range is below that in which the cross section of the $Al^{27}(n,p)Mg^{27}$ reaction becomes significant. For monoenergetic neutrons the total resolution (FWHM) of the system was calculated to be 0.086 Mev at 0.15 Mev and 0.30 Mev at 2.15 Mev. For spectrum measurements of neutrons of energies between 0.15 and 2.15 Mev the resolution (FWHM) is reduced to 0.154 Mev at 0.15 Mev and 0.327 Mev at 2.15 Mev.

A statistically significant experimental verification of the operation of the triton detection system using a fission neutron source failed due to the high proton background arising from high energy neutron (above 2 Mev) reactions in the aluminum incorporated into the system. The upper limit of the detection system capability depends on the threshhold and yield of neutron reactions involving system materials and leading to the production of charged particles.

Use of the system in a reactor environment would be suitable only if sufficient gamma ray shielding could be provided for the semiconductor detector. Gamma rays decrease the resolution of the system and their presence can be tolerated to the extent that the resolution is not effected significantly.

Use of materials, (excepting the "converter" foil) which yield charged particles in the energy range from 1.98 to 4.17 Mev as a result of fast neutron reactions, must be minimized. The limits of the above energy range correspond to the detected energy of tritons resulting from reactions produced by 0.15 and 2.15 Mev neutrons. Materials which must be carefully selected include the backing material for the "converter" foil, the collimating grid and "catcher" foil, and all materials included in the detector itself.

The energy resolution of the system could be improved considerably at low neutron energies by using a different linear amplifier, e.g. ORTEC Model No. 201. The electronic noise in the system used in this work contributes 52 Kev to the total system resolution. This could be reduced to approximately 15 Kev FWHM by utilizing a linear amplifier designed specifically for use with the preamplifier used in this work.

The efficiency of the system could be improved by a factor of 3 without appreciably reducing the total system resolution, assuming that better electronic equipment as discussed above was employed. The increase in efficiency would be due to an increase in the thickness of the "converter" foil. The foil used in this work (155 μgm/cm^2) contributes approximately 23 Kev to the FWHM of the triton peak resulting from thermal neutrons.

Triton energy losses in the aluminum "catcher" foil and in air, as determined experimentally for tritons resulting from thermal neutron reactions, are in good agreement with the calculated energy losses. From Figures 15 and 16 it is seen that the triton peak was shifted 120 channels when the "catcher" foil was inserted into the grid. For a channel width of 8.9 Kev this represents a triton energy loss of 1.06 Mev. The difference in detected triton energy with and without the "catcher" foil (Table 3) was calculated to be 1.04 Mev.

Use of the aluminum "catcher" foil contributes approximately 73 Kev to the FWHM of the triton peak.

RECOMMENDATIONS FOR FURTHER STUDY

It would be highly desirable to test this detection system using monoenergetic neutrons at several different energies within the energy range for which it was designed. This would yield experimental values for the resolution of the system as a function of neutron energy. In addition, this would provide a means of checking the triton energy loss calculations for neutrons above thermal energy. The $Li^7(p,n)Be^7$ and $T(p,n)He^3$ reactions are both suitable for generation of neutrons with energies in the range from 0.15 to 2.15 Mev.

As is seen from Equation 11, the thickness of the depletion region for semiconductor detectors is dependent on the magnitude of the applied voltage and resistivity of the detector material. Cederlund et al. (3) have used this characteristic of these detectors as a means of discriminating between alpha-particles and protons. It would be of interest to determine if this method could be used to discriminate between alpha-particles and tritons. If so, the "catcher" foil could be eliminated from the system with a resulting increase in the total resolution of the system.

An alternate method of discriminating between tritons and alpha-particles would be to use pulse shape discrimination. Different charged particles in the process of being stopped in semiconductor detectors produce pulses of different shapes. Suitable electronic systems can detect these different pulse shapes and thus discrimination can be accomplished. Funsten (11) has demonstrated the usefulness of this method.

Further investigations using a fission spectrum should be made. This would require use of a different backing material for the "converter" foil and different materials for the grid and "catcher" foil. Use of a thicker Li^6F foil in conjunction with better electronics would also be an improvement over the current design.

A more detailed analysis of the efficiency of the system could be completed in order that absolute measurements of the number of neutrons at each energy could be made. The current analysis of efficiency is on a relative basis only.

SYMBOLS EMPLOYED

e - electronic charge

$\mathcal{E}$ - electric field strength

E_{α} - alpha-particle energy

E_{dp} - energy available to the disintegration products of the $Li^6(n,T)He^4$ reaction

E_{γ} - gamma ray energy

E_{max} - maximum energy that can be transferred to an electron in the semiconductor material by a charged particle of mass M_p and energy E_p

E_n - neutron energy

E_p - energy of unspecified charged particle

E_T - triton energy

$f(E)$ - fraction of neutrons of a given energy incident on the Li^6F foil which result in a detectable triton

$\Delta h_{\frac{1}{2}}$ - pulse height interval between the points at which one-half of the maximum occurs

h_{max} - pulse height corresponding to the maximum in the curve

K - Boltzman constant

m_{α} - mass of alpha-particle

m_e - electron mass

m_n - mass of neutron

M_p - mass of unspecified charged particle

m_T - mass of triton

N - total number of electron-hole pairs produced by an incident charged particle

n_n - electron concentration in n-type semiconductor material

n_p - electron concentration in p-type semiconductor material

P_α - momentum of alpha-particle resulting from $Li^6(n,T)He^4$ reaction

P_T - momentum of triton resulting from $Li^6(n,T)He^4$ reaction

Q - Q-value for $Li^6(n,T)He^4$ reaction = 4.78 Mev

q_e - contribution to pulse produced in detector by a charged particle due to collection of electrons

q_n - contribution to pulse produced in detector by a charged particle due to collection of holes

T - temperature in degrees Kelvin

v - velocity of electron

V_a - reverse bias applied to the detector

V_o - barrier-height potential of p-n junction

W_1 - contribution to total pulse height spread due to statistics of electron-hole formation

x_o - depth of depletion region existing in the n-type material

x_1 - depth of depletion region existing in the p-type material

Z - atomic number

δ - total detection system resolution (FWHM)

ϵ - average energy required to produce an electron-hole pair in silicon

K_o - dielectric constant of silicon

λ - carrier drift length

μ_n - electron mobility in n-type semiconductor material

ω - standard deviation in triton energy distribution resulting from reaction produced by monoenergetic neutrons

ϕ - maximum triton scattering angle in laboratory system

ϕ_o - maximum triton scattering angle in center-of-mass system

ρ - resistivity of silicon in the detector

Σ_a - macroscropic absorption cross section

σ_a - microscopic absorption cross section

Σ_s - macroscopic scattering cross section

σ_s - microscopic scattering cross section

$\sigma(\phi_o)$ - cross section for $Li^6(n,T)He^4$ reaction yielding a triton which is detected. Conditions are specified in definition of Θ.

τ - transit time for charge carriers

Θ - maximum angle in the laboratory system into which triton can be scattered and still be detected. This assumes the neutron is incident normal to the Li^6F foil and the reaction takes place on the axis of a grid hole.

Θ_o - in terms of center-of-mass system of coordinates

ξ_{E_p} - standard deviation in number of electron-hole pairs produced in semiconductor detectors by charged particle of energy E_p

BIBLIOGRAPHY

1. Aron, W. A., Hoffman, B. G. and Williams, F. C. Range-energy curves. U.S. Atomic Energy Commission Report AECU-663 (Division of Technical Information Extension, AEC). 1951.

2. Blankenship, J. L., and Borkowski, C. J. Silicon surface-barrier nuclear particle spectrometer. Institute of Radio Engineers Transactions on Nuclear Science NS-7, Nos. 2-3: 190-195. 1960.

3. Cederlund, R., Horn, A. and Scolnick, M. Solid state detector for monitoring 14-Mev neutron production. Nuclear Instruments and Methods 13: 305-308. 1961.

4. Dearnaley, G. Radiation damage effects in semiconductor detectors. Nucleonics 22, No. 7: 78-85. 1964.

5. Dearnaley, G., Ferguson, A. T. G. and Morrison, G. C. Semiconductor fast neutron detectors. Institute of Radio Engineers Transactions on Nuclear Science NS-9, No. 3: 174-180. 1962.

6. Dearnaley, G. and Northrop, D. C. Semiconductor counters for nuclear radiations. New York, N.Y., John Wiley Inc. 1963.

7. Dearnaley, G. and Whitehead, A. B. Semiconductor surface-barrier for nuclear particle detection. Nuclear Instruments and Methods 12: 205-226. 1961.

8. Etherington, Harold, ed. Nuclear engineering handbook. New York, N.Y., McGraw-Hill Book Co., Inc. 1958.

9. Firk, F. W. K., Slaughter, G. G. and Ginther, R. J. An improved Li^6-loaded glass scintillator for neutron detection. Nuclear Instruments and Methods 13: 313-316. 1961.

10. Firk, F. W. K., Whittaker, J. K., Bowey, E. M., Lokan, K. H. and Rae, E. R. A nanosecond neutron time-of-flight system for the Harwell 30 Mev electron linac. Nuclear Instruments and Methods 23: 141-146. 1963.

11. Funsten, Herbert O. Pulse shape discrimination in p-n junction detectors. Institute of Radio Engineers Transactions on Nuclear Science NS-9, No. 3: 190-192. 1962.

12. Furr, Keith A. and Runyon, R. S. A fast neutron spectrometer for reactor flux measurements. Nuclear Instruments and Methods 27: 292-298. 1964.

13. Goldberg, M. D., May, V. M. and Stehn, J. R. Angular distributions in

neutron-induced reactions. 2nd ed. U.S. Atomic Energy Commission Report BNL-400, Vol. 1 (Brookhaven National Lab., Upton, N.Y.). 1962.

14. Kahn, David. The energy loss of protons in metallic foils and mica. Physical Review 90: 503-509. 1953.

15. Keepin, G. R., Jr. and Roberts, J. H. Measurement of fast neutron energies by observations of $Li^6(n,\alpha)H^3$ in photographic emulsions. Review of Scientific Instruments 21: 163-166. 1950.

16. Klingensmith, R. W. The effect of a high radiation environment and gold-silicon charged particle detectors. Institute of Radio Engineers Transactions on Nuclear Science NS-8, No. 1: 112-115. 1961.

17. Love, T. A. and Murray, R. B. The use of surface-barrier diodes for fast neutron spectroscopy. Institute of Radio Engineers Transactions on Nuclear Science NS-8, No. 1: 91-97. 1961.

18. Mayer, J. W. Performance of germanium and silicon surface barrier diodes as alpha-particle spectrometers. Journal of Applied Physics 30: 1937-1944. 1959.

19. Mayer, J. W. and Gossick, B. Use of au-ge broad area barrier as alpha-particle spectrometer. Review of Scientific Instruments 27: 407-408. 1956.

20. McKay, K. G. A germanium counter. Physical Review 76: 1537. 1949.

21. McKenzie, J. and Bromley, D. A. Observation of charged-particle reaction products. Physical Review Letters 2: 303-305. 1959.

22. Murray, R. B. Use of Li^6 (Eu) as a scintillation detector and spectrometer for fast neutrons. Nuclear Instruments and Methods 2: 237-248. 1958.

23. Orman, C., Fan, H. Y., Goldsmith, G. J. and Lark-Horovitz, K. Germanium p-n barriers as counters. Physical Review 78: 646. 1950.

24. Potenza, R. and Rubbino, A. Fast neutron spectrometer. Nuclear Instruments and Methods 25: 77-88. 1963.

25. Potenza, R. and Rubbino, A. Spectrometers for fast neutrons from nuclear reactions and from collimated beams. Nuclear Instruments and Methods 26: 93-103. 1964.

26. Price, W. J. Nuclear radiation detection. 2nd ed. New York, N.Y., McGraw-Hill Book Co., Inc. 1964.

27. Rybakov, B. V. and Sidorov, B. A. Fast-neutron spectroscopy. Soviet Journal of Atomic Energy Supplement No. 6: 1-121. 1958.

28. Wolke, R. L., Bishop, W. N., Eichler, E., Johnson, N. R. and O'Kelley, G. D. Range and stopping cross section of tritons. Physical Review 129: 2591-2596. 1963.

ACKNOWLEDGEMENTS

The author wishes to thank Dr. D. M. Roberts for suggesting this problem and assisting throughout the investigation and preparation of the thesis.

Gratitude is also extended to the Atomic Energy Commission and to the Babcock and Wilcox Company for loaning the fission foils.

In addition, appreciation is extended to those members of the nuclear engineering staff who operated and supervised the operation of the UTR-10 reactor during the experimental portion of this work.

APPENDIX A

Equipment List

1. Detector .... ORTEC* Model No. NHD300 CO, Surface-barrier type: Area = 300 mm^2, Resistivity = 3000 ohm-cm
2. Power Supply .... ORTEC Model No. 106, Serial No. 49
3. Preamplifier .... ORTEC Model No. 105, Serial No. 190
4. Linear Amplifier .... RIDL. This device was an integral part of the 400 channel analyzer.
5. 400 Channel Analyzer..... RIDL Model No. 34-12B, Serial No. 84611 C
6. Pulse Generator.......... RIDL Model No. 47-7, Serial No. 50E8429
7. Alpha-particle source ... Am^{241} $E_{\alpha} = 5.477$ Mev, Prepared by ORTEC
8. Fission Foils .... 1 inch diameter, 0.020 inch thick, 93% enriched in U-235

---

* Oak Ridge Technical Enterprises Corporation

APPENDIX B

Discussion of Lead-Cadmium Foil

The lead-cadmium foil used in this work was designed to replace two of the 1 inch diameter, 0.020 inch thick fission foils. The appropriate cross section and density data, used in making the calculations to determine the amounts of lead and cadmium needed in the foil, are listed below.

Cd	$\Sigma_a = 114\ cm^{-1}$,	$\Sigma_s = 0.325\ cm^{-1}$,	density = $8.65\ \frac{gm}{cm^3}$
Pb	$\Sigma_a = 0.006\ cm^{-1}$,	$\Sigma_s = 0.363\ cm^{-1}$,	density = $11.35\ \frac{gm}{cm^3}$
U^{235}	$\sigma_a = 683$ barns,	$\sigma_s = 10$ barns,	density = $19\ \frac{gm}{cm^3}$
U^{238}	$\sigma_a = 2.7$ barns,	$\sigma_s = 8.3$ barns,	density = $19\ \frac{gm}{cm^3}$

The amounts of lead and cadmium required in the foil were determined as follows:

1. The macroscopic absorption and scattering cross sections were calculated for the fission foils. The calculated values were $\Sigma_a = 30.860\ cm^{-1}$ and $\Sigma_s = 0.480\ cm^{-1}$.
2. The total absorption and scattering cross sections of the two fission foils was calculated by multiplying the volume of the foils by Σ_a and Σ_s respectively. The total absorption cross section was calculated to be $15.90\ cm^2$ and the total scattering cross section was calculated to be $0.247\ cm^2$.
3. The amount of cadmium required to provide the same total absorption

cross section as the two fission foils was calculated to be $0.1395\ cm^3$ or 1.164 gms. It was assumed that lead would make no contribution to the absorbing properties of the foil.

4. The contribution of 1.164 gms of cadmium to the total scattering cross section of the foil was calculated to be $0.0452\ cm^2$.
5. The difference between the total scattering cross section of the fission foils and the contribution to this provided by the cadmium was calculated to be $0.2018\ cm^2$.
6. The amount of lead required to provide this total scattering cross section was calculated to be $0.556\ cm^3$ or 6.32 gms.

The lead-cadmium foil was made by melting the appropriate mass ratio of lead and cadmium and pouring the melt into a graphite mold. The 1 inch diameter foil was then machined until the total mass required (6.32 gms of lead + 1.164 gms of cadmium = 7.484 gms) was attained.

APPENDIX C

Data

Table 7. Energy resolution of pulse generator output

Date: March 25, 1966 | Temperature: 24°C
Reactor Power Level: | Counting Time:

Analyzer Settings: Conversion Gain: 1 | Course Gain: $\frac{1}{4}$ | Fine Gain: 69
Threshold: 120 | Upper Level: 1100 | Store-In: 0-400

Pulse Generator Setting: Pulse Height: 1.62 | Attenuation: 5x | Polarity: -
Normalize: 0

Detector Power Supply: Detector Bias: 30 volts

Preamplifier Settings: Gain: x1 | Invert: X | Non-Invert:

Channel Number	1	2	3	4	5	6	7	8	9	10
01-10	00000	00000	00002	00000	00000	00000	00000	00000	00000	00000
11-20	00000	00000	00000	00000	00000	00000	00000	00000	00000	00000
21-30	00000	00000	00000	00000	00000	00000	00001	00000	00000	00000
31-40	00000	00000	00000	00000	00000	00000	00000	00000	00000	00000
41-50	00001	00002	00009	00021	00050	00164	00278	00512	00750	00922
51-60	01012	00974	00777	00552	00308	00143	00079	00037	00011	00001
61-70	00002	00000	00000	00000	00000	00000	00000	00000	00000	00000
71-80	00000	00000	00001	00000	00000	00000	00000	00000	00000	00000

Table 8. Energy resolution of triton peak produced by thermal neutrons

Date: April 8, 1966 | Temperature: 24°C
Reactor Power Level: 75 watts | Counting Time: 10 min.

Analyzer Settings: Conversion Gain: 1 | Course Gain: $\frac{1}{4}$ | Fine Gain: 69
Threshold: 50 | Upper Level: 1100 | Store-In: 0-400

Pulse Generator Setting: Pulse Height: | Attenuation: 5x | Polarity: -
Normalize: 0

Detector Power Supply: Detector Bias: 30 volts

Preamplifier Settings: Gain: x1 | Invert: X | Non-Invert:

Channel Number	1	2	3	4	5	6	7	8	9	10
61-70	00055	00063	00051	00043	00075	00063	00051	00084	00073	00060
71-80	00065	00070	00088	00087	00096	00111	00104	00132	00110	00119
81-90	00139	00132	00146	00137	00190	00177	00210	00199	00234	00212
91-100	00229	00263	00259	00253	00254	00258	00299	00303	00325	00284
101-110	00279	00322	00290	00322	00319	00308	00297	00305	00311	00320
111-120	00320	00307	00300	00304	00321	00311	00308	00264	00296	00263
121-130	00256	00244	00214	00406	00190	00180	00156	00128	00126	00092
131-140	00094	00055	00043	00034	00026	00019	00012	00006	00004	00001
141-150	00005	00003	00003	00003	00001	00001	00001	00004	00001	00007
151-160	00003	00004	00004	00003	00005	00006	00004	00004	00004	00001
161-170	00001	00004	00004	00004	00003	00009	00005	00005	00002	00001
171-180	00003	00004	00000	00005	00007	00003	00002	00004	00002	00005
181-190	00001	00002	00001	00003	00004	00005	00003	00003	00005	00004
191-200	00004	00007	00005	00002	00007	00005	00005	00005	00003	00005
201-210	00009	00005	00009	00007	00008	00007	00010	00008	00007	00010
211-220	00018	00021	00018	00025	00022	00031	00028	00033	00043	00037
221-230	00042	00056	00052	00059	00046	00078	00085	00092	00133	00179
231-240	00253	00333	00475	00681	00833	01085	01211	01301	01374	01306
241-250	01112	00931	00710	00508	00301	00163	00093	00032	00017	00008
251-260	00003	00003	00001	00002	00000	00000	00000	00001	00003	00001

Table 9. Energy resolution of triton peak produced by thermal neutrons with "catcher" foil in place

---

Date: April 8, 1966 — Temperature: 24°C

Reactor Power Level: 75 watts — Counting Time: 27 min.

Analyzer Settings:	Conversion Gain: 1	Course Gain: $\frac{1}{4}$ Fine Gain: 69
	Threshold: 50	Upper Level: 1100 Store-In: 0-400
Pulse Generator Setting:	Pulse Height:	Attenuation: 5x Polarity: -
	Normalize: 0	
Detector Power Supply:	Detector Bias: 30 volts	
Preamplifier Settings:	Gain: x1	Invert: X Non-Invert:

Channel Number	1	2	3	4	5	6	7	8	9	10
81-90	00047	00051	00052	00043	00046	00062	00062	00070	00064	00091
91-100	00071	00095	00109	00097	00132	00140	00152	00173	00191	00215
101-110	00241	00271	00278	00286	00401	00358	00393	00456	00528	00528
111-120	00685	00666	00709	00758	00793	00803	00850	00914	00937	00865
121-130	00829	00711	00679	00599	00536	00504	00383	00330	00275	00190
131-140	00177	00141	00080	00060	00036	00028	00017	00018	00014	00010
141-150	00006	00007	00006	00001	00003	00002	00002	00005	00007	00000
151-160	00003	00004	00001	00003	00002	00003	00003	00002	00002	00002
161-170	00003	00001	00000	00002	00001	00002	00000	00002	00001	00002

Table 10. Results obtained with detection system inside thermal column at point 32 inches from "south" core tank

Date: March 8, 1966 | Temperature: $23^{\circ}C$

Reactor Power Level: 300 watts | Counting Time: 10 min.

Analyzer Settings: Conversion Gain: 1 | Course Gain: $\frac{1}{4}$ | Fine Gain: 69

Threshold: 120 | Upper Level: 1100 | Store-In: 0-400

Pulse Generator Setting: Pulse Height: | Attenuation: | Polarity: -

Normalize: 0

Detector Power Supply: Detector Bias: 30 volts

Preamplifier Settings: Gain: x1 | Invert: X | Non-Invert:

Channel Number	1	2	3	4	5	6	7	8	9	10
01-10	00000	00001	00000	00000	00001	00000	00009	00157	00093	00056
11-20	00076	00095	00083	00134	00117	00130	00145	00136	00171	00193
21-30	00225	00245	00267	00307	00375	00437	00510	00578	00630	00682
31-40	00786	00841	00993	01058	01193	01279	01467	01515	01770	01873
41-50	02099	02185	02260	02596	02783	02868	03109	03387	03552	03815
51-60	03915	04183	04393	04425	04744	04857	05174	05288	05477	05651
61-70	05750	05835	05820	06123	06121	06320	06286	06346	06284	06366
71-80	06441	06402	06380	06393	06171	06183	06048	06171	05794	05987
81-90	05812	05653	05571	05401	05261	05175	05104	04994	04866	04715
91-100	04487	04500	04247	04107	04110	03966	03807	03683	03514	03396
101-110	03303	03211	03016	02971	02822	02797	02709	02673	02536	02439
111-120	02361	02245	02124	02039	02063	01871	01790	01746	01816	01669
121-130	01696	01584	01468	01433	01415	01398	01331	01234	01231	01187
131-140	01112	01062	01048	01043	00983	00918	00809	00846	00814	00781
141-150	00778	00791	00705	00692	00713	00642	00604	00639	00585	00590
151-160	00559	00548	00481	00456	00480	00417	00422	00398	00392	00373
161-170	00348	00322	00346	00305	00337	00310	00311	00260	00247	00275
171-180	00262	00221	00229	00235	00203	00194	00202	00205	00228	00179
181-190	00165	00172	00184	00152	00159	00136	00126	00149	00142	00102
191-200	00108	00116	00115	00112	00088	00109	00090	00088	00093	00088

Table 11. Results obtained with detection system inside thermal column at point 46 inches from "south" core tank (Used one fission foil)

Date: March 11, 1966		Temperature: $27^{\circ}C$			
Reactor Power Level: 600 watts		Counting Time: 15 min.			
Analyzer Settings:	Conversion Gain: 1	Course Gain: $\frac{1}{4}$		Fine Gain: 69	
	Threshold: 120	Upper Level: 1100		Store-In: 0-400	
Pulse Generator Setting:	Pulse Height:	Attenuation:		Polarity: -	
	Normalize: 0				
Detector Power Supply:	Detector Bias: 30 volts				
Preamplifier Settings:	Gain: x1	Invert: X		Non-Invert:	

Channel Number	1	2	3	4	5	6	7	8	9	10
01-10	00000	00002	00000	00000	00001	00000	00000	00002	00027	00019
11-20	00016	00022	00016	00017	00029	00026	00022	00049	00054	00043
21-30	00053	00061	00082	00080	00124	00151	00158	00150	00202	00240
31-40	00304	00322	00361	00422	00446	00513	00592	00651	00747	00811
41-50	00907	01000	01057	01172	01347	01427	01485	01672	01762	01858
51-60	01928	02092	02203	02311	02477	02487	02730	02629	02839	02947
61-70	03022	03124	03141	03222	03245	03176	03160	03286	03251	03382
71-80	03285	03349	03125	03215	03251	03063	02987	03073	02886	02838
81-90	02870	02647	02666	02528	02395	02453	02404	02224	02160	02110
91-100	02046	01963	01872	01801	01813	01645	01600	01563	01500	01471
101-110	01370	01336	01295	01204	01148	01079	01063	01013	00985	00940
111-120	00854	00859	00817	00815	00819	00710	00675	00669	00649	00563
121-130	00578	00573	00550	00549	00501	00501	00454	00445	00426	00410
131-140	00349	00391	00349	00285	00332	00305	00322	00286	00258	00260
141-150	00245	00244	00228	00226	00207	00207	00185	00192	00185	00168
151-160	00134	00174	00149	00156	00143	00122	00116	00121	00145	00121
161-170	00109	00115	00078	00103	00088	00104	00091	00096	00081	00070
171-180	00073	00068	00071	00063	00050	00073	00057	00046	00063	00057
181-190	00054	00050	00049	00066	00045	00051	00045	00036	00035	00038
191-200	00036	00041	00033	00032	00032	00022	00032	00017	00025	00039

Table 12. Results obtained with detection system inside thermal column at point 46 inches from "south" core tank (No fission foil used)

Date: March 11, 1966 | Temperature: 27°C
Reactor Power Level: 600 watts | Counting Time: 8 min.

Analyzer Settings:	Conversion Gain: 1 Threshold: 120	Course Gain: $\frac{1}{4}$ Upper Level: 1100	Fine Gain: 69 Store-In: 0-400
Pulse Generator Setting:	Pulse Height: Normalize: 0	Attenuation:	Polarity: -
Detector Power Supply:	Detector Bias: 30 volts		
Preamplifier Settings:	Gain: x1	Invert: X	Non-Invert:

Channel Number	1	2	3	4	5	6	7	8	9	10
01-10	00000	00000	00000	00000	00001	00000	00001	00009	00004	00008
11-20	00005	00003	00007	00006	00007	00004	00015	00014	00011	00022
21-30	00021	00026	00029	00038	00054	00051	00058	00093	00098	00107
31-40	00112	00137	00147	00195	00223	00217	00279	00311	00357	00396
41-50	00472	00514	00551	00644	00654	00691	00816	00920	00937	01044
51-60	01064	01130	01154	01291	01371	01366	01458	01596	01592	01577
61-70	01691	01605	01775	01820	01797	01851	01799	01834	01791	01832
71-80	01861	01778	01871	01805	01748	01758	01628	01606	01612	01566
81-90	01576	01501	01459	01408	01305	01321	01237	01209	01193	01150
91-100	01070	01069	01044	00983	00952	00902	00842	00837	00793	00713
101-110	00727	00757	00678	00647	00596	00573	00597	00538	00467	00463
111-120	00476	00456	00436	00411	00397	00344	00417	00337	00325	00332
121-130	00266	00312	00313	00244	00264	00239	00212	00223	00200	00205
131-140	00207	00200	00160	00180	00163	00162	00136	00145	00137	00117
141-150	00116	00115	00094	00110	00085	00096	00080	00086	00075	00092
151-160	00071	00082	00073	00057	00061	00064	00065	00054	00039	00051
161-170	00050	00051	00048	00046	00033	00033	00028	00029	00034	00024
171-180	00030	00028	00024	00026	00025	00029	00022	00021	00022	00019
181-190	00022	00020	00023	00018	00019	00014	00013	00007	00020	00015
191-200	00010	00012	00012	00008	00006	00008	00007	00008	00007	00006

Table 13. Resolution of pulse generator output at reactor power levels of 0 and 5000 watts

Date: March 29, 1966		Temperature: 23.8°C	
Reactor Power Level: 0 and 5000 watts		Counting Time:	
Analyzer Settings:	Conversion Gain: 1 Threshold: 110	Course Gain: $\frac{1}{4}$ Upper Level: 1100	Fine Gain: 69 Store-In: 0-400
Pulse Generator Setting:	Pulse Height: 3.60, 4.04 Normalize: 0	Attenuation: 5x	Polarity: -
Detector Power Supply:	Detector Bias: 30 volts		
Preamplifier Settings:	Gain: x1	Invert: X	Non-Invert:

Channel Number	1	2	3	4	5	6	7	8	9	10
271-280	00000	00000	00000	00001	00002	00006	00013	00020	00052	00085
281-290	00157	00360	00790	01246	01402	01322	01063	00796	00519	00241
291-300	00162	00073	00039	00007	00001	00002	00000	00000	00000	00000
301-310	00000	00000	00000	00000	00001	00000	00001	00000	00000	00001
311-320	00003	00010	00015	00016	00021	00019	00037	00059	00055	00081
321-330	00112	00146	00193	00197	00241	00299	00279	00345	00343	00301
331-340	00347	00313	00274	00283	00295	00251	00258	00232	00241	00201
341-350	00172	00149	00159	00130	00143	00146	00089	00106	00102	00096
351-360	00090	00087	00073	00059	00065	00063	00052	00049	00055	00041
361-370	00044	00033	00046	00040	00035	00034	00033	00027	00029	00016
371-380	00023	00024	00021	00024	00016	00015	00017	00017	00018	00014

Table 14. Resolution of pulser peaks at different reactor power levels with apparatus positioned as shown on Figure 22

Date: March 29, 1966 | Temperature: 24°C
Reactor Power Level: 0, 100, 500, 1000, 2500 watts | Counting Time:

Analyzer Settings: Conversion Gain: 1 | Course Gain: ¼ | Fine Gain: 69
Threshold: 110 | Upper Level: 1100 | Store-In: 0-400

Pulse Generator Setting: Pulse Height: 2.00, 2.50, 3.00, 3.50, 4.04 | Attenuation: 5x | Polarity: -
Normalize: 0

Detector Power Supply: Detector Bias: 30 volts

Preamplifier Settings: Gain: x1 | Invert: X | Non-Invert:

Channel Number	1	2	3	4	5	6	7	8	9	10
91-100	00002	00004	00002	00002	00001	00001	00005	00000	00001	00001
101-110	00010	00023	00061	00142	00341	00612	01016	01400	01689	01614
111-120	01419	01101	00702	00392	00201	00079	00030	00013	00006	00003
~										
151-160	00000	00000	00001	00005	00016	00028	00103	00235	00443	00832
161-170	01165	01504	01681	01525	01306	00883	00479	00286	00122	00069
171-180	00047	00021	00013	00011	00009	00010	00002	00004	00003	00005
~										
201-210	00001	00000	00000	00000	00000	00001	00000	00004	00006	00016
211-220	00028	00082	00157	00341	00568	00825	01144	01465	01550	01378
221-230	01153	00911	00669	00427	00270	00175	00120	00086	00067	00060
231-240	00041	00046	00037	00034	00016	00011	00012	00023	00018	00009
~										
261-270	00004	00003	00004	00010	00027	00059	00143	00255	00407	00623
271-280	00814	01104	01229	01196	01109	00889	00725	00568	00392	00290
281-290	00212	00187	00113	00107	00079	00084	00059	00058	00052	00039
291-300	00041	00041	00033	00019	00015	00016	00018	00012	00011	00016
~										
321-330	00008	00009	00021	00039	00064	00107	00181	00263	00347	00414
331-340	00571	00639	00700	00745	00726	00748	00647	00563	00498	00455
341-350	00372	00322	00261	00223	00228	00154	00155	00149	00140	00104
351-360	00093	00085	00085	00081	00081	00056	00056	00060	00044	00043
361-370	00034	00030	00032	00036	00025	00023	00021	00017	00018	00015

Table 15. Resolution of pulser peaks at different reactor power levels with apparatus shielded as shown on Figure 25

Date: March 31, 1966 | Temperature: 25°C
Reactor Power Level: 0, 500, 1000, 5000 watts | Counting Time:

Analyzer Settings: Conversion Gain: 1 | Course Gain: $\frac{1}{4}$ | Fine Gain: 69
Threshold: 110 | Upper Level: 1100 | Store-In: 0-400

Pulse Generator Setting: Pulse Height: 2.08, 2.54, 3.08, 3.503 | Attenuation: 5x | Polarity: -
Normalize: 0

Detector Power Supply: Detector Bias: 30 volts

Preamplifier Settings: Gain: x1 | Invert: X | Non-Invert:

Channel Number	1	2	3	4	5	6	7	8	9	10
101-110	00002	00000	00003	00000	00003	00002	00003	00002	00005	00008
111-120	00025	00074	00157	00331	00555	00829	01094	01152	01048	00857
121-130	00580	00352	00180	00077	00034	00008	00001	00000	00000	00000
131-140	00000	00001	00000	00000	00000	00000	00000	00002	00000	00002
141-150	00000	00000	00000	00002	00000	00000	00001	00000	00000	00000
151-160	00000	00000	00000	00001	00000	00001	00000	00001	00000	00002
161-170	00012	00013	00029	00093	00138	00268	00442	00643	00743	00858
171-180	00778	00816	00674	00426	00322	00212	00170	00103	00075	00076
181-190	00044	00038	00033	00030	00017	00030	00019	00013	00007	00015
191-200	00010	00011	00008	00012	00008	00007	00005	00010	00002	00008
201-210	00003	00008	00006	00007	00003	00002	00003	00002	00001	00001
211-220	00000	00000	00002	00004	00001	00000	00001	00001	00010	00009
221-230	00022	00040	00107	00165	00274	00392	00525	00650	00670	00698
231-240	00672	00578	00429	00329	00256	00218	00165	00117	00110	00095
241-250	00087	00080	00067	00051	00044	00034	00030	00030	00040	00023
251-260	00025	00021	00024	00025	00027	00034	00036	00056	00051	00083
261-270	00114	00116	00148	00175	00190	00202	00238	00214	00219	00285
271-280	00229	00261	00224	00231	00240	00223	00217	00209	00192	00199
281-290	00190	00175	00151	00129	00143	00131	00100	00113	00102	00099
291-300	00086	00096	00075	00093	00072	00066	00082	00065	00059	00068
301-310	00055	00055	00049	00043	00042	00041	00037	00033	00030	00023
311-320	00029	00017	00030	00024	00029	00019	00022	00017	00021	00018

Table 16. Resolution of pulser peaks with boral substituted for cadmium

Date: April 2, 1966 | Temperature: $25^{\circ}C$
Reactor Power Level: 0, 500, 1000, 5000 watts | Counting Time: 11 min.

Analyzer Settings: Conversion Gain: 1 | Course Gain: $\frac{1}{4}$ | Fine Gain: 69
Threshold: 110 | Upper Level: 1100 | Store-In: 0-400

Pulse Generator Setting: Pulse Height: 2.08, 2.54, 3.08, 3.50 | Attenuation: 5x | Polarity: -
Normalize: 0

Detector Power Supply: Detector Bias: 30 volts

Preamplifier Settings: Gain: x1 | Invert: X | Non-Invert:

Channel Number	1	2	3	4	5	6	7	8	9	10
21-30	00191	00176	00182	00216	00201	00209	00253	00262	00271	00294
31-40	00313	00357	00358	00392	00455	00503	00506	00568	00578	00665
41-50	00677	00763	00835	00905	00881	00968	00927	00939	00983	00953
51-60	01004	00903	00926	00920	00832	00789	00692	00640	00607	00507
61-70	00450	00375	00337	00268	00229	00200	00153	00129	00109	00124
71-80	00090	00084	00079	00070	00066	00043	00036	00044	00034	00032
81-90	00029	00020	00023	00028	00027	00026	00019	00017	00017	00008
91-100	00012	00013	00007	00018	00010	00007	00010	00007	00006	00003
101-110	00005	00002	00006	00009	00005	00012	00025	00065	00160	00284
111-120	00525	00864	01104	01176	01149	00926	00592	00342	00169	00067
121-130	00034	00009	00003	00003	00002	00002	00003	00001	00001	00000
151-160	00000	00001	00000	00000	00002	00002	00001	00000	00010	00024
161-170	00052	00152	00287	00494	00714	01008	01100	01048	00882	00609
171-180	00412	00217	00092	00056	00036	00014	00013	00012	00007	00004
181-190	00004	00002	00003	00004	00001	00003	00004	00002	00001	00000
211-220	00000	00000	00001	00000	00000	00000	00000	00007	00014	00054
221-230	00100	00211	00362	00573	00859	00968	01006	00910	00771	00527
231-240	00334	00175	00137	00061	00035	00023	00019	00019	00014	00007
261-270	00001	00004	00009	00031	00070	00108	00202	00304	00476	00520
271-280	00711	00740	00727	00664	00502	00424	00315	00246	00175	00165
281-290	00132	00085	00081	00066	00054	00044	00036	00028	00046	00019
291-300	00026	00020	00018	00024	00013	00014	00017	00014	00006	00009

Table 17. Results of run using 2 fission foils, "converter" foil, grid and "catcher" foil

Date: April 28, 1966 | Temperature: 24.5°C
Reactor Power Level: 4000 watts | Counting Time: 53 min.

<u>Analyzer Settings:</u> Conversion Gain: 1 | Course Gain: $\frac{1}{4}$ | Fine Gain: 69
Threshold: 110 | Upper Level: 1100 | Store-In: 0-400

<u>Pulse Generator Setting:</u> Pulse Height: | Attenuation: | Polarity: -
Normalize: 0

<u>Detector Power Supply:</u> Detector Bias: 30 volts

<u>Preamplifier Settings:</u> Gain: x1 | Invert: X | Non-Invert:

Channel Number	1	2	3	4	5	6	7	8	9	10
91-100	00168	00143	00168	00146	00147	00150	00146	00128	00115	00142
101-110	00127	00134	00119	00134	00118	00126	00120	00110	00127	00115
111-120	00113	00116	00091	00116	00123	00108	00095	00127	00112	00125
121-130	00116	00090	00101	00121	00107	00096	00084	00088	00086	00098
131-140	00097	00099	00097	00090	00089	00094	00106	00089	00080	00084
141-150	00087	00087	00102	00094	00082	00079	00086	00075	00085	00067
151-160	00085	00078	00088	00087	00072	00081	00077	00074	00074	00072
161-170	00064	00075	00079	00074	00071	00068	00073	00081	00063	00060
171-180	00070	00054	00062	00080	00070	00067	00063	00063	00064	00056
181-190	00061	00055	00069	00062	00060	00050	00065	00038	00050	00053
191-200	00063	00061	00063	00069	00049	00052	00060	00045	00055	00060
201-210	00055	00051	00057	00051	00055	00026	00033	00056	00043	00041
211-220	00053	00035	00037	00044	00037	00054	00044	00037	00045	00036
221-230	00053	00037	00030	00038	00054	00032	00035	00036	00031	00048
231-240	00050	00038	00038	00041	00045	00028	00025	00033	00051	00031
241-250	00028	00028	00041	00036	00025	00030	00035	00034	00037	00031
251-260	00031	00040	00028	00021	00035	00037	00022	00036	00028	00025
261-270	00027	00032	00029	00027	00031	00023	00031	00024	00030	00024
271-280	00020	00021	00020	00030	00029	00019	00023	00030	00031	00028
281-290	00024	00021	00026	00027	00022	00023	00029	00023	00018	00019
291-300	00020	00019	00018	00017	00020	00021	00025	00021	00017	00024
301-310	00027	00013	00015	00010	00020	00024	00020	00020	00017	00015
311-320	00018	00013	00016	00019	00014	00013	00017	00012	00017	00021
321-330	00008	00015	00015	00010	00014	00021	00012	00010	00010	00009
331-340	00017	00010	00015	00018	00018	00012	00012	00008	00011	00011

Table 18. Results of run using lead-cadmium foil, "converter" foil, grid and "catcher" foil

Date: April 27, 1966 | Temperature: 26°C
Reactor Power Level: 4000 watts | Counting Time: 53 min.

<u>Analyzer Settings:</u> Conversion Gain: 1 | Course Gain: $\frac{1}{4}$ | Fine Gain: 69
Threshold: 110 | Upper Level: 1100 | Store-In: 0-400

<u>Pulse Generator Setting:</u> Pulse Height | Attenuation: | Polarity: -
Normalize: 0

<u>Detector Power Supply:</u> Detector Bias: 30 volts

<u>Preamplifier Settings:</u> Gain: x1 | Invert: X | Non-Invert:

Channel Number	1	2	3	4	5	6	7	8	9	10
91-100	00023	00024	00017	00030	00022	00011	00018	00012	00014	00012
101-110	00011	00010	00010	00008	00014	00009	00010	00006	00008	00006
111-120	00006	00008	00005	00006	00007	00009	00007	00003	00007	00001
121-130	00004	00001	00002	00000	00003	00004	00006	00004	00003	00003
131-140	00003	00003	00002	00003	00002	00004	00005	00000	00002	00003
141-150	00003	00004	00004	00000	00001	00002	00001	00001	00003	00000
151-160	00005	00001	00003	00002	00002	00000	00001	00003	00000	00003
161-170	00002	00002	00002	00003	00001	00002	00001	00001	00004	00002
171-180	00003	00001	00003	00003	00006	00002	00002	00002	00001	00001
181-190	00004	00003	00001	00003	00001	00001	00002	00003	00001	00001
191-200	00000	00000	00004	00002	00002	00002	00002	00002	00000	00002
201-210	00000	00002	00001	00001	00000	00001	00001	00001	00001	00000
211-220	00000	00001	00001	00001	00002	00001	00000	00000	00001	00000
221-230	00000	00001	00000	00000	00001	00000	00001	00000	00000	00000
231-240	00001	00001	00000	00002	00000	00000	00000	00000	00000	00001
241-250	00000	00000	00000	00000	00002	00000	00002	00001	00001	00000
251-260	00000	00000	00001	00000	00000	00001	00000	00000	00000	00000
261-270	00000	00000	00000	00001	00000	00000	00000	00000	00000	00001
271-280	00000	00000	00000	00001	00000	00000	00000	00000	00000	00000
281-290	00000	00000	00000	00000	00000	00000	00000	00000	00001	00000
291-300	00001	00000	00000	00001	00000	00000	00000	00001	00000	00002
301-310	00000	00000	00000	00004	00001	00000	00000	00000	00000	00000
311-320	00000	00001	00001	00000	00000	00000	00000	00001	00000	00000
321-330	00000	00001	00000	00000	00001	00000	00000	00000	00000	00000
331-340	00000	00000	00000	00000	00000	00000	00000	00000	00000	00000

Table 19. Results of run using 2 fission foils, 0.018 inch aluminum, grid and "catcher" foil

Date: April 28, 1966 — Temperature: 25°C
Reactor Power Level: 4000 watts — Counting Time: 53 min.

Analyzer Settings: Conversion Gain: 1; Threshold: 110; Course Gain: $\frac{1}{4}$; Upper Level: 1100; Fine Gain: 69; Store-In: 0-400

Pulse Generator Setting: Pulse Height; Normalize: 0; Attenuation: ; Polarity: -

Detector Power Supply: Detector Bias: 30 volts

Preamplifier Settings: Gain: x1; Invert: X; Non-Invert:

Channel Number	1	2	3	4	5	6	7	8	9	10
91-100	00140	00119	00127	00124	00125	00141	00146	00121	00101	00125
101-110	00110	00122	00105	00127	00112	00111	00125	00105	00103	00110
111-120	00102	00102	00102	00103	00116	00098	00110	00098	00102	00088
121-130	00112	00089	00098	00092	00103	00095	00080	00079	00082	00088
131-140	00090	00079	00094	00082	00074	00075	00072	00093	00076	00077
141-150	00074	00088	00087	00070	00074	00076	00074	00077	00084	00073
151-160	00070	00067	00080	00079	00072	00070	00075	00075	00068	00068
161-170	00065	00070	00072	00073	00070	00070	00073	00079	00067	00060
171-180	00066	00051	00058	00075	00056	00059	00073	00061	00064	00058
181-190	00055	00056	00047	00052	00059	00046	00064	00037	00049	00049
191-200	00056	00050	00050	00045	00045	00047	00060	00048	00052	00050
201-210	00053	00036	00043	00044	00049	00043	00049	00042	00040	00041
211-220	00037	00039	00033	00044	00034	00037	00030	00035	00041	00035
221-230	00031	00024	00030	00036	00035	00038	00043	00038	00032	00044
231-240	00035	00035	00037	00028	00033	00027	00036	00030	00034	00030
241-250	00027	00026	00032	00024	00033	00025	00028	00032	00033	00029
251-260	00017	00026	00019	00023	00022	00032	00032	00032	00027	00020
261-270	00025	00022	00023	00024	00015	00020	00019	00020	00029	00028
271-280	00017	00020	00016	00019	00026	00018	00029	00029	00026	00023
281-290	00022	00015	00023	00020	00022	00015	00017	00020	00017	00018
291-300	00018	00017	00017	00020	00017	00019	00021	00018	00014	00016
301-310	00024	00014	00014	00013	00017	00021	00023	00015	00015	00006
311-320	00016	00019	00014	00016	00014	00016	00020	00012	00014	00015
321-330	00008	00015	00010	00009	00015	00017	00014	00008	00008	00010
331-340	00010	00009	00011	00015	00014	00012	00012	00009	00010	00010